

T 1481

THE DESIGN OF UNDERGROUND EXCAVATIONS
USING THE STIFFNESS CONCEPT

by

Franklin Robinson

ProQuest Number: 10781795

All rights reserved

INFORMATION TO ALL USERS

The quality of this reproduction is dependent upon the quality of the copy submitted.

In the unlikely event that the author did not send a complete manuscript and there are missing pages, these will be noted. Also, if material had to be removed, a note will indicate the deletion.



ProQuest 10781795

Published by ProQuest LLC (2018). Copyright of the Dissertation is held by the Author.

All rights reserved.

This work is protected against unauthorized copying under Title 17, United States Code
Microform Edition © ProQuest LLC.

ProQuest LLC.
789 East Eisenhower Parkway
P.O. Box 1346
Ann Arbor, MI 48106 – 1346

A Thesis submitted to the Faculty and the Board of Trustees of the Colorado School of Mines in partial fulfillment of the requirements for the degree of Master of Science.

Signed: Franklin Robinson
Franklin Robinson

Golden, Colorado

Date: July 3rd, 1972

Approved: William Hustrulid
William Hustrulid
Thesis Advisor

A. M. Keenan
A. M. Keenan
Head of Department

Golden, Colorado

Date: June 9, 1972

LIBRARY
COLORADO SCHOOL OF MINES
GOLDEN, COLORADO

ABSTRACT

A stiff testing machine designed by W. A. Hustrulid and constructed by the C.S.M. Instrument Shop was used to perform all the experimental work presented in this thesis. The required electronic and hydraulic instrumentation of the stiff testing machine was developed, followed by its calibration.

Experiments were made (1) to determine the failure behavior and the complete stress-strain curves of coal measure rocks such as coal, limestone, sandstone, and shale, and (2) to simulate the behavior of pillars in the laboratory and to utilize data in actual mine design.

Axial splitting in the direction of the major principal stress was revealed to be the true failure mode of rock in uniaxial compression. Shear types of failure were observed in unstable processes in which the stiffness of the machine was not high enough to control the fracture propagation.

The effect of the platen restraints became prominent for short specimens, showing a stabilizing effect similar to lateral confining pressures.

Experiments showed an influence of the specimen shape on the slope of the post failure stress-strain curve.

Longer specimens revealed a steeper slope.

Simulation in the computer of a rib-pillar mine showed the importance of knowing the compressive strength of pillars and the relative elastic properties of pillars and host rock to determine the pillar loads and mine stiffnesses.

The manner to input laboratory data into the computer and a design method for mining excavations have been suggested.

CONTENTS

	Page
1. INTRODUCTION	1
2. ROCK FAILURE BEHAVIOR UNDER CONTROLLED LOADING CONDITIONS	4
2.1 Introduction.	4
2.2 Stiff-Testing Machine	7
2.2.1 Principles of Design	7
2.2.2 Design and Instrumentation of the CSM Stiff Testing Machine.	12
2.3 Uniaxial Compression Tests.	15
2.3.1 Rock Types and Sample Preparation.	15
2.3.2 Experimental Procedure	16
2.4 Experimental Result and Discussion	18
2.4.1 Mechanical Behavior of Rock in Uniaxial Compression	18
2.4.2 Fracture Patterns in Uniaxial Compression.	22
2.4.3 Influence of Specimen Size on the Complete Stress-Strain Curve	27
2.4.4 Influence of Specimen Shape on the Complete Stress-Strain Curve	28
2.5 Conclusions	29
3. DESIGN OF UNDERGROUND EXCAVATIONS.	31
3.1 Introduction.	31
3.2 Computer Model.	33
3.3 Input of Laboratory Data into Actual Mine Design	36

	Page
3.4 Examples of Rib Pillar Mine Design.	38
3.4.1 Example No. 1.	38
3.4.2 Example No. 2.	40
3.5 Discussion of Computer Results.	41
3.6 Conclusions	43
3.7 Recommendations for Further Work.	43
REFERENCES	45
FIGURES.	48
APPENDIX A - Determination of the Sample Deformation	89
APPENDIX B - Computer Program to Calculate Pillar Loads and Stiffnesses in a Rib Pillar Mine.	95

LIST OF FIGURES

Figure	Page
1. Picture of the CSM testing machine	48
2. An Oil Shale sample mounted in the stiff testing machine.	48
3. Diagrammatic representation of the stiff testing machine.	49
4. Actual force deformation record when testing a Sandstone sample in the stiff machine; the specimen length is 4 in. and its diameter is 2 in. Several loading-unloading cycles are shown.	50
5. Complete stress-strain curve for Sandstone in uniaxial compression.	51
6. Typical regions of the stress-strain curve in the post-failure zone for the rocks tested in these experiments.	52
7. Complete stress-strain curve for Indiana Limestone in uniaxial compression.	53
8. Polished sections of Indiana Limestone showing state of failure with increased uniaxial loading along the stress-strain curve. The stress-strain curve is shown in Figure 7	54
9. Unconfined Indiana Limestone in advanced stages of failure. Two different shapes and size specimens are shown	58
10. Complete failed samples of Indiana Limestone tested in uniaxial compression	60
11. Sample sections of partially failed Indiana Limestone in uniaxial compression.	61

Figure	Page
12. Typical failure mode of unconfined Indiana Limestone loaded in a conventional testing machine	61
13. Complete stress-strain curve for sandstone in uniaxial compression.	62
14. Polished sections of sandstone showing state of failure with increased uniaxial loading along the stress-strain curve. The stress-strain curve is shown in Figure 13	63
15. Remnants of Oil Shale samples loaded in uniaxial compression	67
16. Complete stress-strain curve for coal in uniaxial compression.	68
17. Series of photographs taken at various points along the stress-strain curve for a coal sample tested in uniaxial compression. The stress-strain curve is shown in Figure 16	69
18. Complete stress-strain curve for coal in uniaxial compression	75
19. Influence of specimen shape on the complete stress-strain curve for Indiana Limestone in uniaxial compression.	76
20. Influence of specimen shape on the complete stress-strain curve for Indiana Limestone in uniaxial compression.	77
21. Influence of specimen shape on the complete stress-strain curve for sandstone in uniaxial compression.	78
22. Influence of specimen shape on the complete stress-strain curve for Oil Shale in uniaxial compression.	79
23. Influence of specimen size on the complete stress-strain curve for Indiana Limestone in uniaxial compression.	80

Figure	Page
24. Influence of specimen size on the complete stress-strain curve for Indiana Limestone in uniaxial compression.	81
25. Influence of specimen size on the complete stress-strain curve for Indiana Limestone in uniaxial compression.	82
26. Influence of specimen size on the complete stress-strain curve for sandstone in uniaxial compression	83
27. Distribution of stresses and stiffnesses for a four-room panel.	84
28. State of stress in the central pillar as mining progresses.	85
29. Variation of the stiffness at the central pillar as mining progresses.	86
30. Layout of the excavation for the second example.	87
31. Variation of stresses with the value of E/E_s	88
32. Variation of the stiffness with the value of E/E_s for a two-room panel	88

LIST OF DIAGRAMS

Diagram	Page
1. Representation of specimen and testing machine.	7
2. Specimen and testing machine characteristics under load.	9
3. Stress-strain curve illustrating the behavior for a soft loading system	10
4. Stress-strain curve illustrating the behavior of a stiff loading system	11
5. Representation of contact and failed zone in a long specimen.	21
6. Stress induced at a strip a distance X from a strip with average convergence S.	34
A-1. Calibration curve of the two DCDTs	93
A-2. Calibration curve of the load cell	94

LIST OF TABLES

Table	Page
1. Experimental results from the unconfined compression tests	17
2. Laboratory results for saturated specimens.	23
3. Stress-strain data for partially failed, unconfined Indiana Limestone.	23
4. Stress-strain data for partially failed, unconfined sandstone.	24
5. Stress-strain data for partially failed, unconfined coal	24

88 3/12/50

ACKNOWLEDGMENTS

The author expresses his gratitude to:

Professor William Hustrulid, thesis advisor, for the suggestions, guidance, and help in the preparation of this investigation,

Professors J. J. Reed and N. Grosvenor for serving on the thesis committee,

Institute of International Education and the Fulbright Commission for their scholarship,

Mr. Paul Wu, graduate student, for his help in the photographic work,

Mr. Raymond Frahm, Mining Department Research Technician, for the assistance during many phases of the experiments.

1. INTRODUCTION

The development of a rational method for the design of underground openings is very important in the planning of a mine. The lack of knowledge concerning the failure processes in rock has led to the development of many design procedures based on the ultimate compressive strength of the rock. Some studies (Cook, 1965a, 1967; Starfield and Fairhurst, 1968; Starfield and Wawersik, 1968; Salamon, 1970) have shown that knowledge of the strength and deformation characteristics of the rock after the peak strength is important to determine the stability of any underground excavation. Whether or not the rock will exhibit this post-failure behavior depends on the conditions and characteristics of the loading system.

Experiments in the laboratory have shown the difference in the failure process of rock specimens when using a conventional testing machine (violent failure) or a stiff testing machine (controlled or stable failure). Observations made in underground mines in which pillars are left for strata control reveal that normally the pillars fail in a controlled fashion and very seldom fail violently. The similarity of loading conditions between a compression machine and the mine area might logically lead us to conclude

that pillars fail violently or in a stable manner depending on the relative stiffnesses of the mine and the pillars.

The choice of a mining method depends not only on the shape and the size of the orebody, but also on the mechanical properties of the ore and the host rock. The shape, dimensions, and sequence in the excavation of an underground mine must be determined according to the ability of the rock to sustain loads after the peak strength has been reached. Knowledge of the complete stress-strain characteristics of rocks is, therefore, a fundamental prerequisite to the optimum design of mining excavations, mainly at great depths.

If the complete stress-strain characteristics of rock are important for the design of a mining excavation, knowledge of the failure mechanism must be an important factor to identify stable and unstable failures in underground mines. Unfortunately, the failure mechanism of rocks is not constant. It depends upon rock composition, moisture, temperature, confining pressure, and especially, on the inhomogeneities contained in the rock mass as jointing, faulting, etc. Due to the difficulty in conducting controlled experiments in-situ, laboratory tests offer an approach to study the failure mechanism of rock. This approximation is considered to be valid due to the similar loading conditions with mine pillars.

Many investigators (Fairhurst and Cook, 1966; Bieniawsky, 1967; Bieniawsky and others, 1969; Rummel and

Fairhurst, 1970) have been conducted during the last 10 years to study the failure mechanism of rock. These efforts have been centralized on the utilization of stiff-testing machines.

This research is divided into an experimental and a theoretical part. In the experimental section, tests using a stiff-testing machine were conducted to determine the complete stress-strain curves of rocks for specimens with different shapes and sizes. An attempt to study the fracture patterns using photography techniques was made for the different rocks. The theoretical section consists of the computer simulation of a rib-pillar mine. Examples are given of how to input experimental data for actual mine design.

2. ROCK FAILURE BEHAVIOR UNDER CONTROLLED LOADING CONDITIONS

2.1 Introduction

The uniaxial strength of rock is generally determined by using an hydraulic jack, and recording the stress at which the jack-specimen system becomes unstable. Some studies (Wawersik, 1968; Hudson and others, 1971b) have shown that only small changes occur in the rock before this ultimate compressive strength has been reached. The large changes and rapid failure processes generally occur when the applied stress becomes equal to the compressive strength. Most rocks show brittle behavior, failing violently and uncontrollably, when compressed in a conventional testing machine. It has now been found that such unstable failure is largely due to the soft or low stiffness characteristics involved in the system. Consequently, control of the failure process can be achieved by increasing the stiffness of the compression machine. Various attempts have been made to control the failure process in rock. Barnard (1964) and Cook (1965b) were the first to show that unstable and rapid failure of a rock sample is merely due to the sudden release of stored energy in the compression machine when the maximum load-carrying ability of the specimen is exceeded.

Bieniawski and others (1969) obtained the complete stress-strain curve of sandstone, quartzite and norite utilizing a compression machine stiffened by means of steel bars in parallel with the rock specimen. Brady and others (1971) used a stiff-loading system similar to the one used by Bieniawsky to study the post-failure characteristics of marble, Mt. Airy granite, Pikes Peak granite, and Texas granite. Wawersik (1968) employed thermal contraction of the machine so as to gradually deform specimens of Tennessee marble, charcoal gray granite, Indiana limestone, basalt, slate, and Solenhofen limestone. Wawersik (1968) found that there is a rock class where failure is unstable or self-sustaining even if an infinitely stiff testing machine is used. Owing to this finding, Rummel and Fairhurst (1970) used a small servo controlled testing machine to determine the post-failure curve of Tennessee marble. All these results have been very important because they showed that violent failure of rock specimens is not an intrinsic rock property, but depends on the design characteristics of the loading system. Those results also showed that brittle materials will retain some strength after the ultimate compressive strength has been exceeded. Thus, determination of the complete stress-strain curve of rock should define the critical curve for material stability. It means that the rock specimen will be stable whenever the energy

supplied by the loading system is not in excess of the energy necessary to produce a determined deformation in the specimen.

Due to the important characteristic of a stiff-testing machine of being stable during the failure processes, the development and joining of cracks can be studied stopping the loading of the rock samples at any desired point in both the pre- and post-failure regions. Only a few attempts have been made to study the development of cracks in the post-failure region. Wawersik (1968) developed the sequence of macroscopic events which occur over the entire deformation curve for several rocks. Wawersik divided the complete stress-strain curve into eight characteristic zones, identifying each one with the extent of fracture in the rock specimen. Rummel and Fairhurst (1970) obtained fracture patterns of unconfined Tennessee marble at different points on the post-failure curve, and Brady and others (1971) stopped the failure processes at selected points along the post-failure curve for marble to obtain the mode of fracture development.

In this part of the research, an attempt is made to study the mechanical behavior and failure process of coal measure rocks in uniaxial compression.

2.2 Stiff-Testing Machine

2.2.1 Principles of Design. A stable rock fracture process depends on the slope of the post-failure curve of the test specimen and on the stiffness of the compression machine. Stiffness of the compression machine is defined by the linear relationship between the force produced by the loading platens and the relative displacement of the platens. The slope of the post-failure curve is the relationship between the load-carrying ability and the displacement of a test sample after its compressive strength has been exceeded.

In order to define the general condition which ensures stability of a test specimen, the loading machine can be represented by a spring with stiffness K_{LM} as shown in Diagram 1.

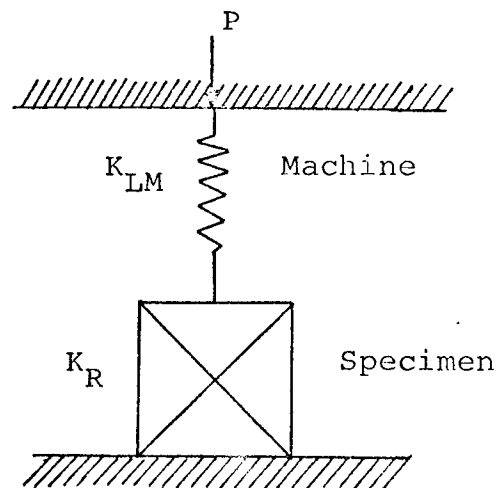


Diagram 1. Representation of specimen and testing machine.

In the pre-failure region (that portion of the stress-strain curve to the left of the peak stress) equilibrium will exist because the load applied by the spring or loading machine is resisted by the rock sample. When the peak stress is reached the rock sample will begin to fail losing the ability to resist loads. At this point, the loading machine will change the direction of deformation releasing the energy, stored during the loading process, against the rock sample. Thus, failure will be stable in the post-failure region (that portion of the stress-strain curve to the right of the peak stress) if the energy released by the loading machine during a differential displacement is smaller than the energy required to produce the same displacement in the rock. The rock in the post-failure can be characterized by a stiffness K_R , the value of which is dependent on both the loading rate and the strain.

According to the statement of stability mentioned before, the condition ensuring stability can be derived in the following manner: If

ΔW_{LM} = energy released by the loading machine during a displacement ΔS , and

ΔW_R = energy required to produce a deformation ΔS in the rock sample,

Then, $\Delta W_{LM} \leq \Delta W_R$, to ensure stability.

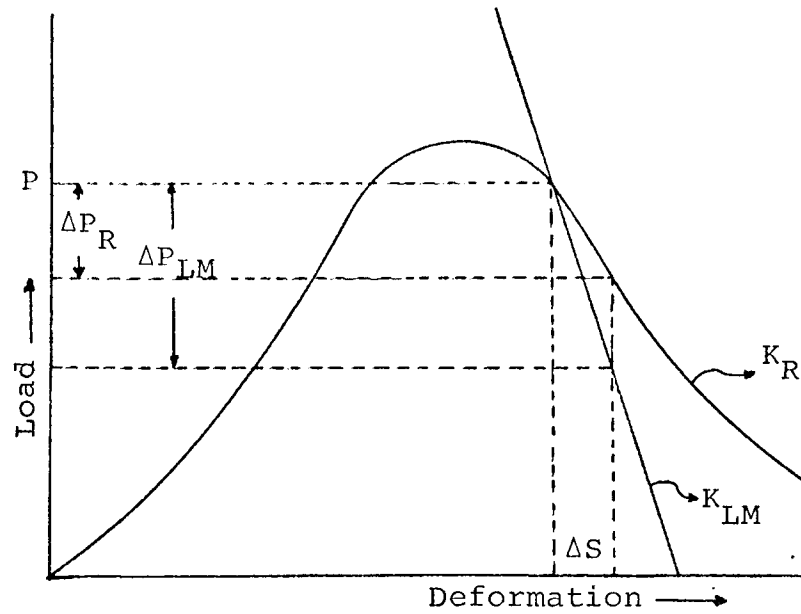


Diagram 2. Specimen and testing machine characteristics under load.

From Diagram 2:

$$\Delta W_{LM} = (P - \frac{1}{2} \Delta P_{LM}) \Delta S \quad (1)$$

$$\Delta W_R = (P - \frac{1}{2} \Delta P_R) \Delta S$$

But

$$\Delta P_{LM} = K_{LM} \Delta S \quad (2)$$

$$\Delta P_R = K_R \Delta S$$

Substituting equation (2) into equation (1), the condition of stability can be written as

$$- \frac{1}{2} K_{LM} \Delta S^2 \leq - \frac{1}{2} K_R \Delta S^2.$$

Eliminating similar values in both sides, one obtains

$$K_{LM} \geq K_R. \quad (3)$$

Equation (3) means that failure will be stable in the post-failure region whenever the slope of the force-displacement

line of the machine is larger or equal to the slope of the force-displacement curve of the rock sample.

In Diagram 3, the machine tries to unload along path 1 and the rock along path 2. For a given change in strain $\Delta \epsilon$, the difference in the areas under the two curves is a measure of the excess energy which accelerates crack growth in the specimen, producing violent failure. This is the general situation for normal testing machines (i.e., the stiffness of the loading system is less than that of the material to be tested).

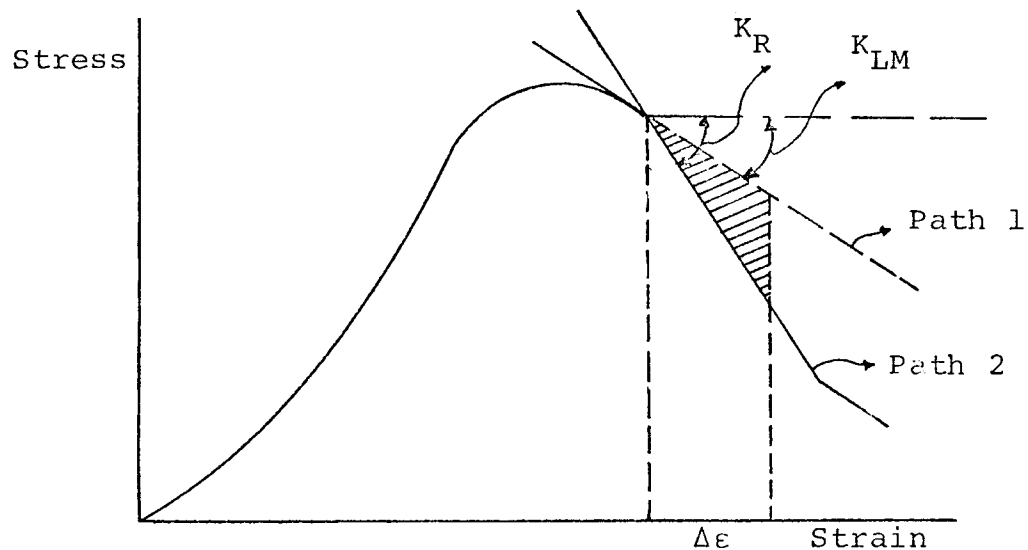


Diagram 3. Stress-strain curve illustrating the behavior of a soft loading system.

The stiff loading system is characterized by a machine stiffness that is larger than that of the rock being tested. This is shown in Diagram 4.

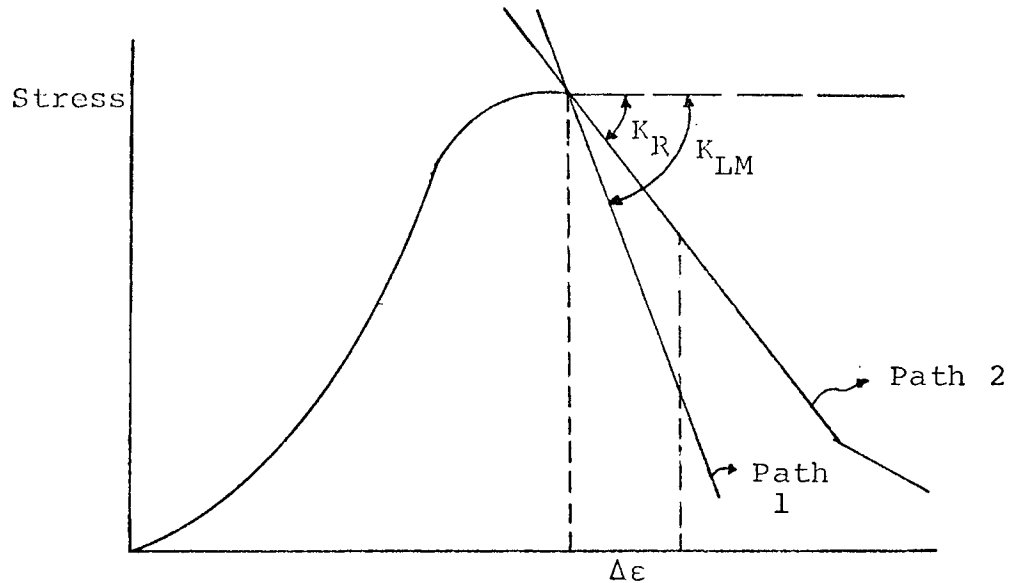


Diagram 4. Stress-strain curve illustrating the behavior of a stiff loading system.

As shown in Diagram 4, energy must be supplied to the machine to produce a displacement of $\Delta \epsilon$ in the rock in the post-failure region. The failure can be carefully studied and controlled in this case. In the CSM stiff-testing machine, which was used in this study, this energy is supplied to the machine by thermally expanding the aluminum upper loading head.

During the past 5 years a number of different so-called 'stiff' loading machines have been developed. The types of machines that have been used include (1) the use of stiffening elements with ordinary large capacity hydraulic loading machines, (2) hybrid machines using various load application methods (including hydraulic and thermal methods), and (3) very fast response (servo controlled) hydraulic machines. The capacities and stiffnesses of these machines vary considerably.

2.2.2 Design and Instrumentation of the CSM Stiff Testing Machine. The machine shown in Figs. 1 and 3 consists of four basic elements:

- (1) the loading frame,
- (2) a hydraulic loading system,
- (3) a thermal loading system,
- (4) a flat-jack clamping system.

The loading frame is constructed from a steel tube 5 ft in length having an outside diameter of 8 inches and a wall thickness of 1 inch. Two windows 8 inches long and 4 inches wide are cut in the upper end of the tube as seen in Fig. 1 to allow the introduction and observation of the samples tested. The window is wide enough to allow use of a small triaxial loading vessel. The ends of the tube are closed with 3" thick steel plates that are bolted around the periphery. Care is taken to insure that the ends are perpendicular to the tube axis. A hole approximately 4 inches in diameter and 1/2 inch deep is bored in the upper side of the base end piece to hold the hydraulic ram.

A 30 ton capacity double acting hydraulic ram (Enerpac type RR-308) is used as the primary loading system. It is set in the recessed region in the base end piece. To the upper end of the ram is axially attached an extension piece 20 inches in length and 3 inches in diameter. The lower platen of the testing machine is screwed to the upper end of this ram extension. Both the upper and lower platens are

2 inches in diameter and are made from hardened steel (58-60 Rockwell C) and are ground flat. The hydraulic connections to the ram are made through holes cut in the wall of the loading frame. An Enerpac pump (type P-84) is used to supply oil to the ram.

The upper loading head consists of three parts. The uppermost piece is an aluminum cylinder 4 inches in diameter and 8 inches long. This is attached to the upper end plate using a 3/4" diameter threaded rod and a nut at the upper side. A bakelite disk 1/2" thick and 4 inches in diameter is then sandwiched between a steel plate 1" thick and 4 inches in diameter and the aluminum cylinder. The lower platen is screwed to this steel disk. A heating tape (Cole-Palmer, type 3106-6, length 6 ft) is wound around the aluminum cylinder with the cord emerging through a hole in the upper end piece. A Cole-Palmer SCR voltage controller is used to heat the tape. Temperatures to 900°F can be generated.

The bakelite sheet was intended to reduce the heat transfer from the cylinder to the upper platen and the sample. It was only partially successful. A cooling coil was made using 1/4" copper tubing and placed between the aluminum head and the inner wall of the loading frame. Cold water is circulated through this during and after testing. The maximum lengthening of the aluminum cylinder when heated is about 110×10^{-6} in./°F. Of course, the

cylinder will shorten due to the increase in load so that the actual lengthening will be less. However, the displacement that can be achieved using even moderate temperature changes is enough to study extensive sections of the post-failure curve of even fairly soft rocks.

A ring of hydraulic 'flat' jacks is situated around the ram extension as can be seen in Fig. 3. They are enclosed in a steel housing that is bolted to an outer cylinder which is in turn bolted to the loading frame. This housing has an inner diameter of 3.005 inches (just sufficient to allow easy travel of the ram). A cross section of the housing is shown in Fig. 3. The inner shell of steel has longitudinal cuts spaced every 45° of arc around the circumference, $1/8$ inches wide and 9 inches long. Pressurization causes the flat jacks to expand against the outer cylinder and the inner shell. The steel shell pushes against the ram extension, thereby fixing it in place. Based on an estimated contact area of 57 sq inches, a jack pressure of 4000 psi, and a coefficient of friction of 0.2, the shear force that can be balanced is about 45,000 lbs. The flat jacks are connected in series to a second hydraulic pump (Enerpac type P-14). The flat jacks were built in the CSM Instrument Shop. The curved frame was made using $1/8$ " diameter steel rod which was covered with 16 gage steel sheets. The edges are heli-arc welded. The travel of the ram is about 5 inches so that a variety of sample lengths can be used.

The load on the specimen is measured using strain gages applied to the lower platen. A complete bridge configuration (two axial and two traverse gages) is used. Ten volts are supplied to the bridge using a Harrison Lab Type 801C power supply. The output is fed into the Y-axis of a Moseley type 7030A X-Y plotter. Calibration is done using a Tinius Olsen testing machine. Specimen deformation is monitored using two DCDTs (type 7DCDT-050). Output from them is summed and fed into the X-axis of the X-Y plotter. Plexiglas blocks mounted on each platen are used to hold the body and the core of the DCDT. Since the position of these blocks are somewhat removed from the specimen ends, the deformations measured include both those of the sample being tested and of a certain length of platen. The method used to obtain the sample deformation alone is given in Appendix A. A plastic sheet is used to seal the area around the lower ram so that the broken material does not fall between the ram and the housing. Power to the DCDTs is supplied using a Harrison Lab Type 801C power supply. Calibration is performed using metal cylinders of known elastic properties as the test samples.

2.3 Uniaxial Compression Tests

2.3.1 Rock Types and Sample Preparation. Four rock types were tested: sandstone, Indiana limestone, oil shale, and coal. It was found that oil shale containing a high

percentage of oil behaves very plastically and because of the large deformation possible it was difficult to fail the material in the stiff testing machine. Oil shale samples with low percentages of oil were therefore chosen for testing.

In order to determine the influence of specimen shape and size on the complete stress-strain curve of rock, specimens with different shapes and sizes (Table 1) were cut and the ends ground parallel to $\pm 1.0 \times 10^{-3}$ ins. Smaller diameter specimens were preferred for oil shale to avoid exceeding the stiffness of the machine. It was not possible to test coal for different L/D values due to the difficulty of cutting specimens longer than 2 in.

2.3.2 Experimental Procedure. The basic idea of the testing system is quite simple. A sample of the rock was first tested in an ordinary testing machine to determine the approximate uniaxial compressive strength. A second sample was then placed between the platens and a load of approximately 90% of this value applied using the hydraulic ram. The valve to the pump was then closed and the pressure to the flat jacks applied (presently about 4000 psi is applied). This essentially locked the lower platen in place. The upper head was then heated using the heat tape. Lengthening of the aluminum cylinder produced a corresponding shortening of the sample. As the sample shortened, the load continued to increase until the compressive strength

Table 1. Experimental results from the unconfined compression tests.

Rock Type	Diam. (inch)	L:D Ratio	Number of Samples	Young's Modulus, E 10 ⁶ psi	Post Failure Slope, Ep 10 ⁶ psi	Post Failure Slope, 10 ⁶ lbs/inch	Ep/E	Uniaxial Compr. Strength, Cp (psi)
	2.0	2:1	4	3.79	-2.91	-2.29	0.769	5700.0
	2.0	1.5:1	4	3.72	-2.26	-2.37	0.608	6423.0
Indiana	2.0	1:1	3	3.61	-1.24	-1.94	0.342	6910.0
Limestone	1.5	2.5:1	2	3.99	-4.90	-2.00	1.230	6000.0
	1.5	2:1	2	3.75	-3.16	-1.90	0.840	6400.0
	1.5	1.5:1	2	3.54	-2.21	-1.72	0.625	6450.0
	1.5	1:1	3	3.34	-1.93	-1.73	0.581	6500.0
	2.0	2:1	3	1.98	-3.31	-2.59	1.110	7510.0
Sandstone	1.25	2:1	3	2.54	-5.55	-2.72	2.18	9190.0
	1.25	3:1	2	2.30	-8.70	-2.84	3.78	7643.0
	0.825	2.5:1	3	2.71	-5.68	-1.52	2.152	18820.0
Oil Shale	0.825	3:1	4	2.62	-7.12	-1.54	2.730	16210.0
	0.825	3.5:1	3	2.65	-10.15	-1.80	3.830	14870.0
	2.0	1:1	1	0.148	-0.392	-0.535	2.656	1240.0
Coal	2.0	1:1	1	0.196	----	----	----	1980.0
	2.0	1:1	1	0.166	-0.280	-0.364	1.69	1380.0

was reached, and then decreased with continued deformation. Cold water was passed through the coils during the experiment. For some samples the failure process was stopped at a series of points in the post-failure region to determine the fracture patterns in partially failed rock specimens. Frequently, the specimens were unloaded and reloaded at various points along the post-failure curve to control in a better manner the failure process. Partially fractured specimens were cast in hydrostone and sectioned. The specimen sections were then polished and photographed.

The stiffness of the compression machine is about 2.0×10^6 lbs/in. This value was determined by placing a hydraulic jack between the platens and applying a force against the machine. The stiffness was then calculated as the ratio of the force and the relative displacement of the platens. From the slope of the force-deformation curves obtained in the laboratory, the system stiffness is at least 2.4×10^6 lbs/in.

2.4 Experimental Results and Discussion

2.4.1 Mechanical Behavior of Rock in Uniaxial Compression. An actual force-displacement record when testing a sandstone specimen is shown in Fig. 4. This is not the true force-displacement curve for the sample since the deformation of the platens is included also. This deformation must

be determined as described in Appendix A and the 'true' curve for the sample derived. The 'corrected' stress-strain curve derived from the force-displacement curve of Fig. 4 is shown in Fig. 5.

All the rocks tested in this study showed a similar behavior in the rising portion of the stress-strain curve. No visible fracture development was observed before the compressive strength was reached, except for coal where failure started at about 75% of the maximum compressive strength. For the rocks tested, similar mechanical behavior in the post-failure curve was observed. They fall in the category of Class I as defined by Wawersik (1968). Three characteristic regions (Fig. 6) can be inferred from the behavior of the four types of rock after the ultimate compressive strength has been reached. Region A is characterized by a flat-falling portion that marks the transition between the maximum compressive strength and region B. The shape of the force-deformation curves reveals that the supporting area is not reduced considerably in region A. This is observed by the photographs of sample sections taken in this region (Figs. 8 and 14). The large reduction in supporting area is observed from the photographs to be located in region B. A constant slope runs through this region which accounts for an 80-90% reduction of the load-carrying ability for specimens with a length to diameter

ratio (L/D) equal or larger than one. The constant slope suggests that these rock types have a uniform failure process in region B. An exception was observed in coal, where the slope was very variable. This is seen in Fig. 16, where the vertical jumps were caused by sudden failures or reductions in supporting area. There is no doubt that this is a characteristic of failure in coal, and is not caused by a lack of stiffness in the compression machine. Region C was only recorded when the length to diameter ratio (L/D) of the rock sample was less than 1.5. For specimens with a L/D value larger than 1.5, a complete failure took place in a more or less unstable manner, before reaching region C. This phenomenon could be explained using two concepts:

- (1) in general, the failure zone is concentrated in the central part of the specimen's length due to lateral restraints at the specimen ends (Hudson and others, 1971b). Then, if the specimen is divided into a failed zone and an elastically loaded zone (Diagram 5), the stiffness of the loading system (machine plus intact rock) must be less than the true stiffness of the machine alone, prompting the unstable failure of the specimen in the central part, and
- (2) the stress-strain curve becomes steeper when the length to diameter ratio of the specimen increases (Starfield and Wawersik, 1968; Hudson and others, 1971b).

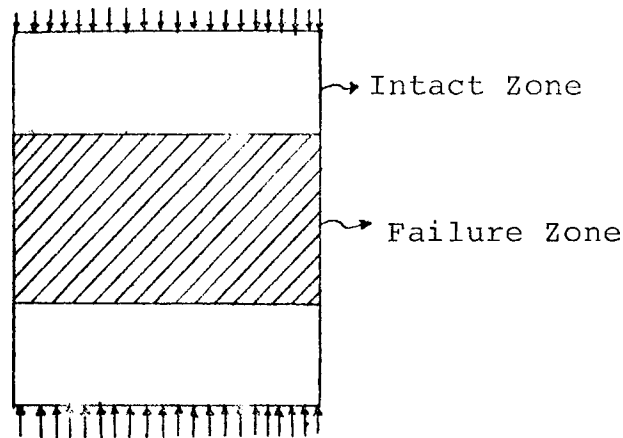


Diagram 5. Representation of intact and failed zone in a long specimen.

These two factors should act together to prompt unstable failure on specimens with a $L/D > 1.5$ when the stiffness of the machine is not high enough.

For short specimens ($L/D \leq 1$), the failure zone appeared to be distributed throughout the length of the specimen. One explanation of this behavior consists in the presence of a more or less uniform confining stress throughout the specimen due to the interaction of the upper- and lower-platens end restraints. The intact and failed zones can be seen in Fig. 9 (a) to (d), for long and short specimens.

It is apparent from Figs. 19 to 21 that any decrease of L/D resulted in an increase of the load-carrying ability of the rock sample in region C. This phenomenon is similar to the results obtained by Bieniawski and others (1969), and

Wawersik (1968) when applying confining pressures to the specimen.

It is important to mention that partially failed specimens still exhibited elastic properties (Wawersik, 1968). From Fig. 5, it is observed that if the load is reduced at any point along the falling portion of the stress-strain curve, elastic strain energy is recovered.

Tests on saturated samples showed no influence of moisture content on the post-failure curve compared with that for dry specimens (Table 2).

In Table 1 are summarized the results of the laboratory tests for the four rock types of this investigation.

2.4.2 Fracture Patterns in Uniaxial Compression. The development of fracture patterns were studied for sandstone, Indiana limestone, and coal. The fracture patterns in these rocks are best recognized in the series of photographs, Figs. 8, 14, and 17. For Indiana limestone and sandstone, polished sections of samples which were loaded from zero stress to the stress-strain values listed in Tables 3 and 4 and indicated in Figures 8 (a) to (d) and 14 (a) to (d), respectively are shown. For coal, the photographs show samples loaded in the stiff compression machine, from zero stress to the stress-strain values listed in Table 5 and indicated in Fig. 17 (a) to (k). From the photographs it is seen that the propagation of cracks is very similar for

Table 2. Laboratory results for saturated specimens.

<u>Rock Type</u>	<u>Diam. (in.)</u>	<u>L:D Ratio</u>	<u>Young's Modulus, E 10⁶ psi</u>	<u>Post Failure Slope, Ep 10⁶ psi</u>	<u>Uniaxial Comp. Strength, Cp (psi)</u>
Sandstone	2.0	2:1	1.910	3.200	4940.0
	2.0	1:1	1.320	1.400	5670.0
Indiana Limestone	2.0	1.5:1	3.530	1.800	5330.0
	2.0	1:1	2.900	1.150	6200.0

Table 3. Stress-strain data for partially failed, unconfined Indiana Limestone.

<u>Location on the Curve</u>	<u>Stress (psi)</u>	<u>Strain 10⁻⁴ in./in.</u>
a	6800	30.2
b	6000	36.8
c	4000	50.6
d	2400	65.0

Table 4. Stress-strain data for partially failed, unconfined sandstone.

<u>Location on the Curve</u>	<u>Stress (psi)</u>	<u>Strain 10^{-4} in./in.</u>
a	9000	53.1
b	8400	56.7
c	6600	59.5
d	3600	63.9

Table 5. Stress-strain data for partially failed, unconfined coal.

<u>Location on the Curve</u>	<u>Stress (psi)</u>	<u>Strain 10^{-4} in./in.</u>
a	0.0	0.0
b	1135.0	86.0
c	1190.0	89.5
d	1315.0	98.0
e	1360.0	103.0
f	1370.0	114.0
g	1270.0	119.5
h	1090.0	122.5
i	775.0	131.3
j	300.0	150.0
k	275.0	206.5

Indiana limestone and sandstone, although sandstone showed a more stable failure process. This can be explained by the inhomogeneity and high variation in grain-size present in sandstone (Krynine and Judd, 1957). Wawersik (1968) found also that fine-grained specimens tended to fail in an unstable manner.

Region A marked the formation of incipient slabs formed by cracks parallel to the direction of maximum stress. The most reasonable explanation of this mode of fracture initiation is based on the extension of Griffith flaws in a compressive stress field (Fairhurst and Cook, 1966). Crack growth is inhibited by the minimum compressive stress, and therefore the slabs are most pronounced near the sides of the sample where the confining stress tends to zero. If σ_1 is the major principal stress and σ_3 is the minor principal stress, then there must be a minimum value of the relation σ_1/σ_3 in which cracks are not possible to propagate due to the confining effect of σ_3 . Consequently, cracks are inhibited from propagating into the cones beneath the platens because of the end restraints imposed. Of course, this effect would be a function of the relative E and ν values of the platens and rock.

Region B is marked by collapse of the incipient slabs generated in region A. This phenomenon is explained by Fairhurst and Cook (1966) with the theory of buckling according to Euler relations. Indiana limestone and sandstone

showed similar fracture patterns in this zone. Instability for long specimens ($L/D > 1$) was always associated with a shear failure, either a conical or a line crack extending across the specimen (Fig. 10). In Fig. 11, it is shown two Indiana limestone samples loaded in the stiff-compression machine. The failure was stable at the initiation of region B, but became an unstable process with further applied loading. The same mode of failure resulted when an Indiana limestone specimen was tested in a conventional testing machine (Fig. 12). For short specimens complete collapse was possible only after large strains. This is because cracks are inhibited in the central part of the specimen, due to the confining effect of the ends, and much more strain is necessary to continue fracture propagation until shear failure can occur (Fig. 8).

Fig. 9 (a) to (d) shows samples of Indiana limestone in advanced stages of failure. They point out the difference in the failure mode for two different specimen sizes and shapes. The even manner in which fracture progressed in most of the tests is an indication of the quality in the sample preparation and of the good alignment of the machine during the loading process. The failure process in oil shale was more difficult to control. This can be explained by the fine-grained structure of this rock in which a stable fracture by slabbing is more difficult to develop (Wawersik, 1968). Fig. 15 (a) and (b) show

oil shale samples after complete failure. The fracture patterns were similar to those for Indiana limestone and sandstone, although the slabs were thicker for oil shale. It is important to note that the cores for oil shale were drilled parallel to the bedding planes.

In coal, fractures started before the compressive strength was reached. Slabbing from the sides of the specimen was the common mode of failure. In the post-failure region the occurrence of small bursts was observed, but failure was in a stable manner. In region C, the specimen behaved as a plastic material. The mode of failure for the small specimens of coal tested in this study was very similar to that observed in the in-situ test made by Bieniawski (1967) on a 5 ft cube coal specimen. If the shape of the complete stress-strain curve is determined mainly by the mechanism of progressive structural breakdown of the rock (Hudson and others, 1971b), then it must be similar for both large and small specimens with the same length to diameter ratio.

2.4.3 Influence of Specimen Size on the Complete Stress-Strain Curve. The influence of specimen size on the complete stress-strain curves for Indiana limestone and sandstone is shown in Figs. 23 to 26, deriving the curves for specimens with different diameter and the same L/D value. Figs. 23 to 25 show that there is no significant influence of specimen size on the complete stress-strain

curve (scaled by the original area of the specimen) for Indiana limestone. This is true for the limited range of specimen sizes tested in these experiments. The variations on sandstone were possibly caused because samples were drilled from different blocks. The shape of the complete stress-strain curve is produced by the mechanism of progressive structural breakdown of the test specimens (Hudson and others, 1971b). In this study, the different specimen sizes showed a similar breakdown process, this explaining the small variation in the shape of the complete stress-strain curve.

The compressive strength data indicated that there is no significant compressive-strength size effect for Indiana limestone. It is very likely that the specimens, for the size range tested in this investigation, are free of pre-existing microfracturing.

2.4.4 Influence of Specimen Shape on the Complete Stress-Strain Curve. Complete stress-strain curves (derived from the force-displacement diagrams) for Indiana limestone, sandstone, oil shale, and coal are shown in Figs. 18 to 22. The influence of specimen shape on the complete stress-strain curve for Indiana limestone, sandstone, and oil shale is shown in Figs. 19 to 22, deriving the curves for different length to diameter ratio (L/D). The shape of the complete stress-strain curve was found to depend upon the shape

of the specimen. In all cases, a more gentle slope of the descending part of the complete stress-strain curve was associated with specimens having a smaller L/D ratio. This variation is mainly caused by the difference in fracture patterns between short and long specimens (Fig. 9). In long specimens ($L/D > 1$), the axial cracks are concentrated in the central part of the specimen's length because lateral restraint of the ends inhibits their growth near the specimen platen interface (Hudson and others, 1971b). In short specimens ($L/D \leq 1$) the cracks appeared to be more uniformly distributed throughout the length of the specimen (Fig. 9 (a) and (e)).

It is possible, for very short specimens, that the stress-strain curve (scaled by the original area) approaches a horizontal line after the peak strength has been reached. In this case, the curve would be very close to the 'true' stress-strain curve defined by Brady and others (1971). The apparent plastic behavior in the post-failure region for very short specimens suggests that the supporting area is not reduced, mainly because the restraint of the end suppresses the formation of slabs.

2.5 Conclusions

The following conclusions can be drawn.

1. A stiff-testing machine has been developed and

successfully used to obtain complete stress-strain curves for four rock types.

2. The Young's modulus did not vary with specimen shape or size.

3. Long specimens showed an unstable failure behavior, different from short specimens in which a significant stabilizing effect was observed when end constraints became prominent.

4. Fracturing in the direction of the major principal stress was the true failure mode of rock in compression. Early shear failure was always observed in unstable processes when the stiffness of the machine was not high enough.

5. No major fracture development was observed in the pre-failure region.

6. Fine-grained and homogeneous materials showed a more unstable failure process than inhomogeneous and variable grain size rocks.

7. A significant compressive strength variation was observed with specimen shape. The strength increased when decreasing L/D.

8. The slope of the post-failure curve varied with specimen shape. Larger L/D ratio specimens were associated with steeper slopes.

3. DESIGN OF UNDERGROUND EXCAVATIONS

3.1 Introduction

Rock surrounding underground excavations often fractures during mining. Methods to control fractured rock due to relaxation have been developed successfully. Problems in mining arise when abrupt collapses of the rock take place. These sudden failures can take the form of a rockburst, a violent failure of a pillar, or a violent fall of the roof, etc. When this kind of failure occurs, the mine is classified as unstable and represents one of the more serious hazards for miners and the operation in general. Due to this problem, research to find the cause of instability in a mine has been carried out over the last few years. Cook (1965a) was the first to suggest the application of the complete stress-strain curve of rock either for rockburst or pillar stability. Starfield and Fairhurst (1968) made an analysis of pillar stability in some detail. Salamon (1970) deduced general mathematical criteria for stability or instability, and Starfield and Wawersik (1968) outlined in more detail how laboratory and computer results can be joined to predict stability of the mine.

Although differing greatly in size, there is a direct analogy between a rock sample and an underground pillar (Starfield and Fairhurst, 1968). The axial loading and end

restraints both for pillars and rock samples make the loading conditions similar. The room and pillar sizes together with the rock properties determine the mine stiffness. Consequently, the relative sizes of the rooms and pillars can be adjusted so that the mine stiffness (corresponding to the stiffness of the compression machine) is greater than the slope of the post-failure curve of the pillars. In this situation, the pillar failure takes place in a stable fashion. The complete stress-strain data are therefore needed for the development of a rational method of mine design.

Determination of the complete stress-strain curve for mine pillars introduces many difficulties. It is therefore important to study the behavior of rock in laboratory tests using a stiff-compression machine and under similar loading conditions. If laboratory tests are to be useful in predicting the behavior of mine pillars, the strength of the specimens must be related to the strength of pillars underground and the post-failure characteristics of the laboratory specimens must be the same as those of the mine pillars which they are to model (Starfield and Wawersik, 1968). The strength of mine pillars and laboratory specimens have been shown to be very different (Bieniawsky, 1967, 1968). Laboratory tests can only be of practical value if the strength of the pillars can be predicted from their results. Because the post-failure properties of rock are principally a function of the induced fracture patterns which, in turn,

are governed by the initial stress distribution throughout the pillar or specimen and, therefore, by the boundary conditions which are approximately similar in both cases, it does not seem at all unrealistic to consider a laboratory specimen as a pillar model and to consider the post-failure curves to be similar (Starfield and Wawersik, 1968). Of course, more experimental work would be necessary to check the validity of this theory.

In this part of the thesis a rib pillar mine is simulated in the computer and pillar loads and mine stiffnesses are calculated taking into account the complete stress-strain curves of the pillars. Suggestions as to how the laboratory data can be incorporated into actual mine design are given; and finally, two worked examples show how the pillar loads and mine stiffnesses depend on the relative properties of the host rock and pillars and on the mine geometry.

3.2 Computer Model

A rib-pillar mine was simulated in the computer to determine loads, displacements, and stiffnesses as mining is progressing. The mathematical solution for this simple case was taken from Starfield and Wawersik (1968) and Salamon (1963). The average stress, induced at a strip a distance X from a strip where the average convergence is S , is (Diagram 6):

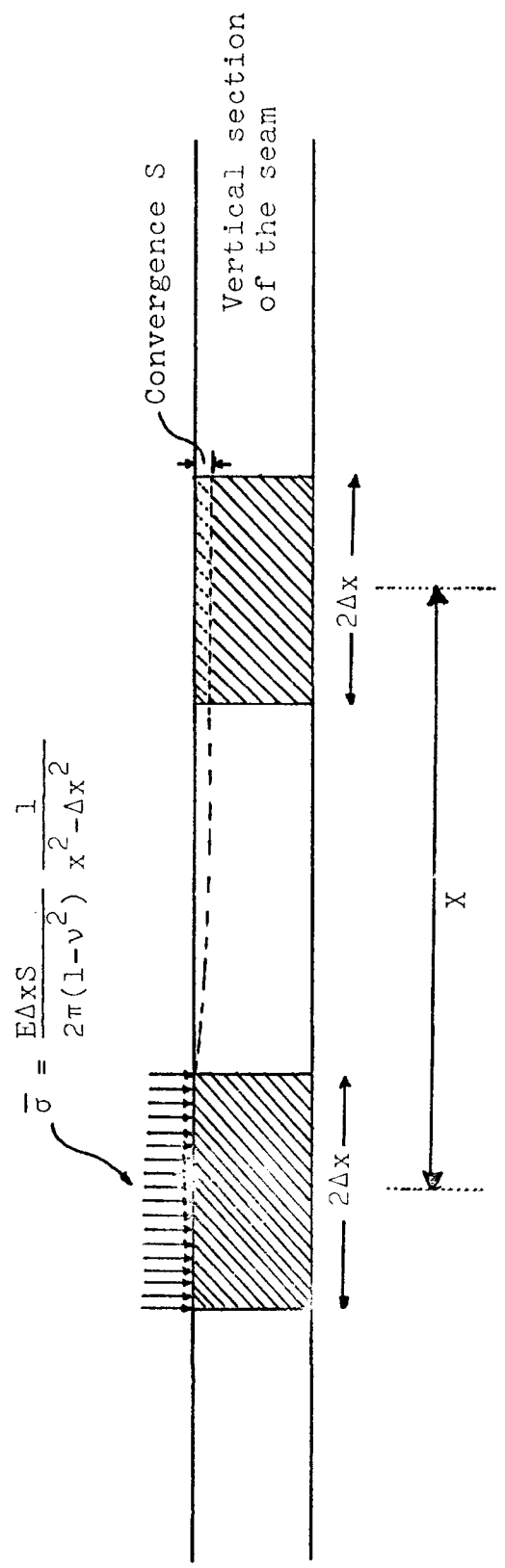


Diagram 6. Stress induced at a strip a distance X from a strip with average convergence S.

$$\bar{\sigma} = \frac{E \Delta x S}{2\pi(1-\nu^2)} \frac{1}{x^2 - \Delta x^2} \quad (1)$$

If the entire area of the seam affected by mining is divided into N strips of width $2\Delta x$, and S_1, S_2, \dots, S_N are the convergences between roof and floor of each strip, then the stress induced at the j^{th} strip by the convergence S_K at the K^{th} strip is obtained by replacing $S = S_K$ and $x^2 = 4(J-K)^2\Delta x^2$ in equation (1). If the stresses induced at the j^{th} strip by the convergences S_1 to S_N are summed, one obtains the total stress induced at j^{th} strips as a result of mining:

$$\sigma_j = \frac{E}{2\pi(1-\nu^2) \Delta x} \sum_{k=1}^N \frac{S_K}{4(J-K)^2 - 1} \quad (2)$$

The convergences S_1 to S_N are not known, but the following relationships must be satisfied by each of the N strips:

1. If Q is the vertical primitive stress, for mined strips

$$\sigma_j = -Q \quad (3)$$

2. If the strip represents a portion of a pillar or abutment

$$\sigma_j = f(S_j/t) \quad (4)$$

where t = thickness of the seam. If pillars and abutments deform in a linearly elastic manner, equation (4) can be written

$$\sigma_j = E_s S_j/t \quad (5)$$

where E_s is Young's modulus for the pillars and abutments.

Equations (2), (3), and (5) produce a set of N linear-simultaneous equations for the N unknown convergences. Having calculated the convergences, the induced stress at any strip can be computed using equation (2).

The stiffness, at any point in the mine, can be determined by increasing the convergence by a small specified amount ΔS_j and then, again using equations (2), (3), and (5), the increase in stress $\Delta \sigma_j$ can be found.

The mine stiffness will be given by:

$$K = t\Delta\sigma_j/\Delta S_j . \quad (6)$$

Equation (6) is given in pounds per square inch.

It was assumed that the rock surrounding the orebody behaves as a homogeneous, isotropic, linearly elastic with Young's modulus E and Poisson's ratio ν .

The computer program to calculate loads and stiffnesses can be seen in Appendix B. It follows the same order of calculation as explained before. The solution of the system of linear-simultaneous equations is done using the Gauss-Seidel iteration method.

3.3 Input of Laboratory Data into Actual Mine Design

The suggestions mentioned here are given mainly for the design of a rib-pillar mine. The direction of mining operations is considered an axis of plane strain. Other extensions of the problem such as the three dimensional case,

transversely isotropic behavior of the host rock, two or more seams at different levels, etc., could be studied with some modification.

The physical properties of the host rock and seam that must be known, before any attempt to design the excavations, are:

- E - Young's modulus of the host rock, considered as being isotropic
- ν - Poisson's ratio of the host rock
- E_s - Young's modulus of the material in the seam
- C_p - Compressive strength of the pillars
- E_p - Slope of the post-failure region of the stress-strain curve of the pillars.

Other variables that must be determined are:

- Q - vertical primitive stress
- T - thickness of the seam.

The physical properties can be determined in the laboratory. Loading conditions must be the same in the laboratory and in-situ. Thus, the tests performed in this study can model the case when roof and floor coincide with natural bedding planes inducing lateral stresses due to frictional end restraint. Different loading conditions can be simulated in the laboratory varying the manner in which load is applied on the specimen.

After the physical properties are found in the laboratory, they must be adjusted to the size of the pillar in-situ.

The compressive strength of pillars can be determined using Holland's formula (Holland, 1964) or Salamon's formula (Salamon, 1967), in the case of coal pillars. The complete stress-strain curve to use must be one determined from a specimen with the same length diameter ratio of the pillar to be designed.

With the mentioned available data, possible geometric configurations according to the size of the seam must be drawn. Roof spans between pillars should be designed to avoid localized roof failure. The abutments and panel are then divided into strips. It was observed that when the strip width became smaller, results were more accurate. Actually, a 5-ft strip width was used for the examples given in the next section. The width of the abutment was enlarged until no major changes in the results were observed.

The mine configuration can be changed very easily until the best one is selected taking into consideration stability and extraction factors.

One of the advantages of using the computer to simulate mine layouts is that variations in the properties of the pillars (the complete stress-strain curve) can be considered. The manner in which the data is input into the computer can be seen in the computer program presented in Appendix B.

3.4 Examples of Rib Pillar Mine Design

3.4.1 Example No. 1. This example will show how

failing or not failing pillars would affect the mine stiffness. The input data are:

$$E = 2.0 \times 10^6 \text{ psi}$$

$$E_s = 2.0 \times 10^6 \text{ psi}$$

$$E_p = -0.2 \times 10^6 \text{ psi}$$

$$\nu = 0.25$$

$$T = 8.0 \text{ ft}$$

$$Q = 1600 \text{ psi}$$

The dimensions of the rooms and pillars are shown in Fig. 27.

The same example was solved for two different compressive strengths of the pillars, 3000 psi and 6000 psi. The panel was widened until 5 rooms were formed.

Figure 27 indicates how the results from loads and stiffnesses are distributed for a 4-room panel. Only half of the panel is shown because the results are symmetrical about the center of the panel.

In Fig. 28 (a) and (b), equilibrium in the central pillar was reached at the points marked on the complete stress-strain curve. When the strength was 3000 psi, failure of the pillars started since two rooms were mined out. For a strength of 6000 psi, pillars did not fail when five rooms were completed.

The variation of the stiffness at the central pillar for the above compression strength is illustrated in Fig. 29 (a) and (b).

3.4.2 Example No. 2. This example shows how the pillar loads and mine stiffnesses depend on the relative properties of the host rock and pillars. The input data are:

$$E = \text{varying from } 3.8 \times 10^6 \text{ to } 1.0 \times 10^6 \text{ psi}$$

$$E_s = 0.2 \times 10^6 \text{ psi}$$

$$E_p = -0.4 \times 10^6 \text{ psi}$$

$$\nu = 0.25$$

$$T = 10 \text{ ft}$$

$$Q = 1000 \text{ psi}$$

$$C_p = 2000 \text{ psi}$$

Room and pillar dimensions are indicated in Fig. 30.

The loads are plotted in Fig. 31 for different ratios of the modulus of the host rock to the modulus of the pillars (E/E_s), and show how the pillar loads depend on the relative elastic properties of the pillars and host rock.

In Fig. 32, the mine stiffness at the central pillar of a two room panel is plotted against E/E_s . It can be noted that the mine stiffness depends on the relative elastic properties of the pillars and host rock. The pillar was always in the pre-failure region.

All these results are valid for narrow panels. If the mine were extended infinitely, the load on each pillar would be the maximum possible calculated as a function of the extraction ratio.

3.5 Discussion of Computer Results

Complete stress-strain curves (scaled by the original area) are very valuable for the design of underground excavations. They assume a decrease in stress corresponding to a decrease in total force when multiplied by the original area. This will simulate the behavior in real conditions in which the total force is decreasing when the pillar is failing. If the true stress-strain curve (Brady and others, 1971) were used, the effective area of the pillar at each stage in the failure process would have to be known. The determination of this effective area would be very difficult. For these reasons, the use of complete stress-strain curves (scaled by the original area) are better justified for the design of underground excavations.

It is seen from Fig. 29 (a) and (b) how important it is to know the compressive strength of the pillars. When the pillars are loaded in the region after the peak strength (Fig. 28 (a)), any increase of the panel width makes the stiffness decrease in the fashion represented by the curve in Fig. 29 (a). If the pillars are not failing (Fig. 28 (b)), the stiffness will follow an almost horizontal path when increasing the panel width (Fig. 29 (b)).

It is very important to know the relative elastic properties of the host rock and pillars. As the relative E/E_s increases, the loads applied on the pillars will become smaller (Fig. 31). The stiffnesses for a given panel

width increase with the value of E/E_s (Fig. 32).

From the results of these examples it can be inferred that a panel can be widened until the smaller mine stiffness is just slightly higher than the slope of the post-failure curve of the pillars. A slope safety factor can be introduced as follows:

$$K \geq FE_p \quad (7)$$

where K = mine stiffness,

E_p = slope of the post-failure curve of the pillars,

F = safety factor of slope.

When the critical point stated by equation (7) is reached, a new panel can be mined out, but leaving a barrier pillar between the two panels. This barrier pillar should be wide enough to eliminate the effect of pillar-panel failures from one panel to another. The design of the barrier pillars should be based on the maximum compressive strength of the pillars. If the barrier pillars failed, the load would then be transferred to neighboring pillars and the stiffness of the entire mine would decrease. These two actions can result in an unstable failure of the entire mine.

It is seen (Fig. 27) that if wider pillars were left at the center of the panel and smaller ones closer to the abutment, a better distribution of loads would be possible. This would delay the failure of the central pillars and consequently wider panels could be mined out before the critical condition stated by equation (7) was reached.

3.6 Conclusions

From the preceding study the following conclusions were reached:

1. Computers can be used as an aid to predict stability or instability in a mine using the data obtained in laboratory tests.

2. Stability of the mine is an important factor to achieve an efficient extraction of minerals. Maximum extraction and safety are the main advantages of using the stiffness concept as a design criteria.

3. The computer model showed the interaction between all the components of a mine. A movement caused by a failure or elastic deformation in any point of the mine will induce deformations throughout the mine, depending on the distance from the source of movement.

4. A design method has been suggested based on the stability condition.

5. The pillar loads and mine stiffnesses depend on the relative elastic properties of the host rock and pillars.

3.7 Recommendations for Further Work

A comparison of computer predictions with real situations in mines should be made. A comparison of laboratory and field failure mechanisms would be very important for better interpretation of laboratory tests. At the same time, field measurements should be made to compare the state of

failure in the mine with computer results of stability or instability. Following various attempts, an adjustment of computer models and the development of general design principles can be formulated.

REFERENCES

- Agapito, J. F., 1972, Pillar design in competent bedded formations: Ph.D. Thesis, Colorado School of Mines.
- Barnard, P. R., 1964, Researches into the complete stress-strain curve for concrete: Mag. Concrete Res., v. 16, no. 49.
- Bieniawski, Z. T., 1967, Mechanism of brittle fracture of rock: CSIR Report, Meg. 580, Pretoria 1967; Int. Jour. Rock Mech. Min. Sci., v. 4, no. 4, p. 395-430.
- _____ 1968, The effect of specimen size on compressive strength of coal: Int. Jour. Rock Mech. Min. Sci., v. 5, p. 325-335.
- _____ 1970, Time-dependent behavior of fractured rock: Rock Mechanics, v. 2, no. 3, p. 123-137.
- Bieniawski, Z. T., Denkhaus, H. G., and Vogler, U. W., 1969, Failure of fractured rock: Int. Jour. Rock Mech. Min. Sci., v. 6, no. 3, p. 323-341.
- Brady, B. T., Duvall, W. I., and Horino, F. G., 1971, A study of the post-failure characteristics of brittle rock: Symposium on Rock Mechanics, Nancy, France.
- Cook, N.G.W., 1965a, A note on rockburst considered as a problem of stability: Jour. S. Afr. Inst. Min. Metall., v. 65, p. 437-446.
- _____ 1965b, The failure of rock: Int. Jour. Rock Mech. Min. Sci., v. 2, p. 389-403.
- _____ 1967, Contribution to discussion: Jour. S. Afr. Inst. Min. Metall., v. 68, p. 192-195.
- Fairhurst, C., and Cook, N.G.W., 1966, The phenomenon of rock splitting parallel to the direction of maximum compression in the neighborhood of a surface: Proc. 1st Congr. Int. Soc. Rock Mech., Lisbon, p. 687-691.
- Holland, C. T., 1964, The strength of coal in mine pillars: Proc. 6th Symp. Rock Mech., Rolla, Mo.

- Hudson, J. A., Brown, E. T., and Fairhurst, C., 1971a, A method of optimizing the control of rock failure in servo-controlled laboratory tests: *Rock Mechanics* (in press).
- _____ 1971b, Shape of the complete stress-strain curve for rock: 13th Symp. on Rock Mech., Urbana, Illinois.
- Hustrulid, W., and Robinson, F., 1972, The design and use of an inexpensive stiff machine for testing rock in compression: To be presented at the 14th Symposium on Rock Mechanics in Pennsylvania State University.
- Krynine, D. P., and Judd, W. R., 1957, Principles of engineering geology and geotechnics: New York, McGraw-Hill, 730 p.
- Rummel, F., and Fairhurst, C., 1970, Determination of the post-failure behavior of brittle rock using a servo-controlled testing machine: *Rock Mechanics*, v. 2, p. 189-204.
- Salamon, M. G. D., 1963, Elastic analysis of displacements and stresses induced by the mining of seam or reef deposits: *Jour. S. Afr. Inst. Min. Metall.*, v. 64, p. 128-149.
- _____ 1967, A method of designing bord and pillar workings: *Jour. S. Afr. Inst. Min. Metall.*, v. 68, p. 68-78.
- _____ 1970, Stability, instability, and design of pillar workings: *Int. Jour. Rock Mech. Min. Sci.*, v. 7, p. 613-631.
- Salamon, M. D. G., and Munro, A. H., 1967, A study of the strength of coal pillars: *Jour. S. Afr. Inst. Min. Metall.*, v. 68, p. 55-67.
- Starfield, A. M., and Fairhurst, C., 1968, How high-speed computer advance design of practical mine pillar systems: *Engng Min. Jour.*, v. 169, p. 78-84.
- Starfield, A. M., and Wawersik, W. R., 1968, Pillars as structural components in room and pillar mine design: *Proc. 10th Symp. Rock Mech.*, Univ. of Texas.
- Wawersik, W. R., 1968, Detailed analysis of rock failure in laboratory compression tests: Ph.D. Thesis, University of Minnesota.

Wawersik, W. R., and Fairhurst, C., 1970, A study of brittle rock fracture in laboratory compression experiments:
Int. Jour. Rock Mech. Min. Sci., v. 7, no. 5, p. 561-575.

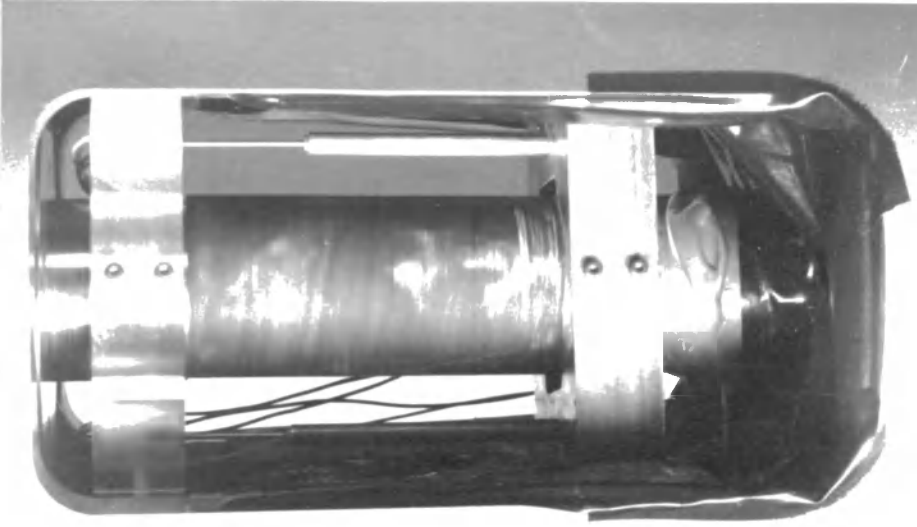


Figure 2. An oil shale sample mounted in the stiff testing machine.

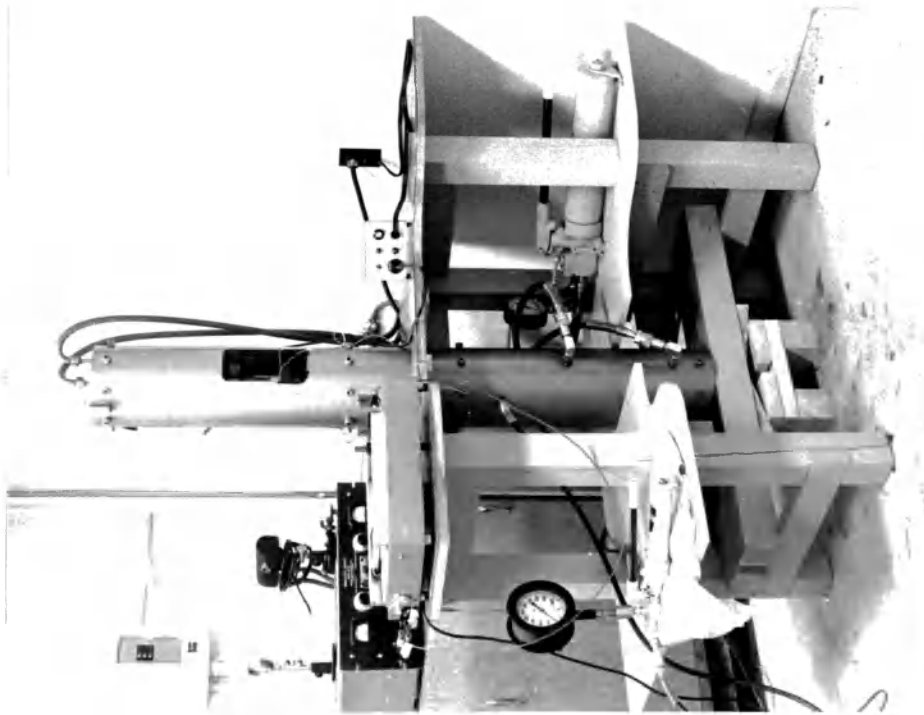


Figure 1. Picture of the CSM stiff testing machine.

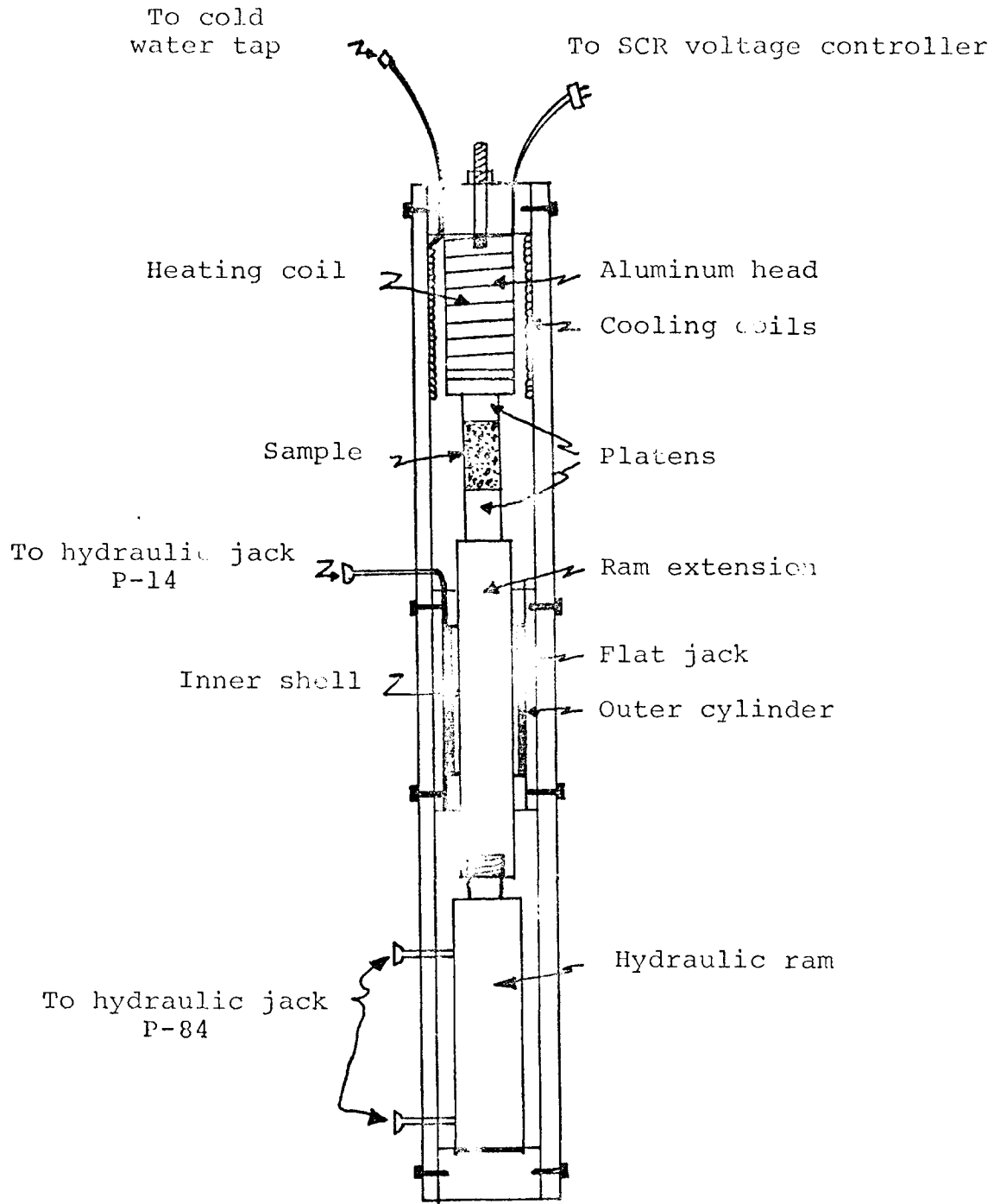


Figure 3. Diagrammatic representation of the stiff testing machine.

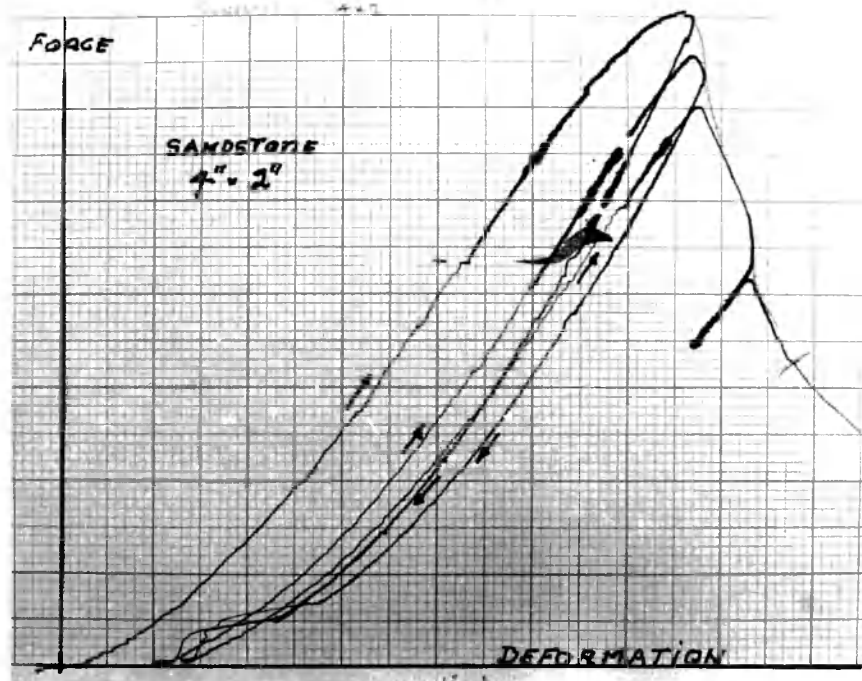


Figure 4. Actual force-deformation record obtained when testing a sandstone sample in the stiff machine; the specimen length is 4 in. and its diameter is 2 in. Several loading-unloading cycles are shown.

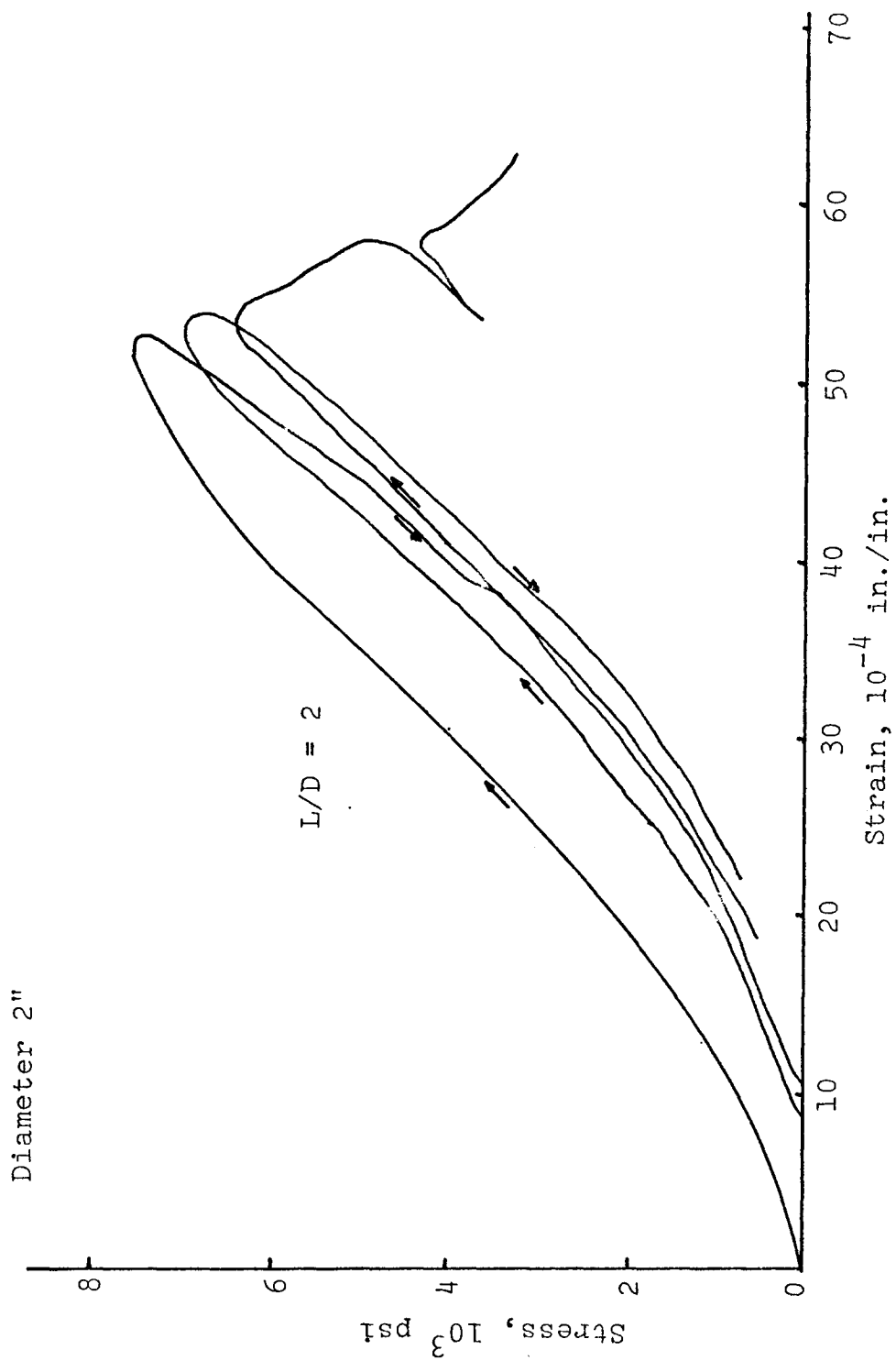


Figure 5. Complete stress-strain curve for sandstone in uniaxial compression.

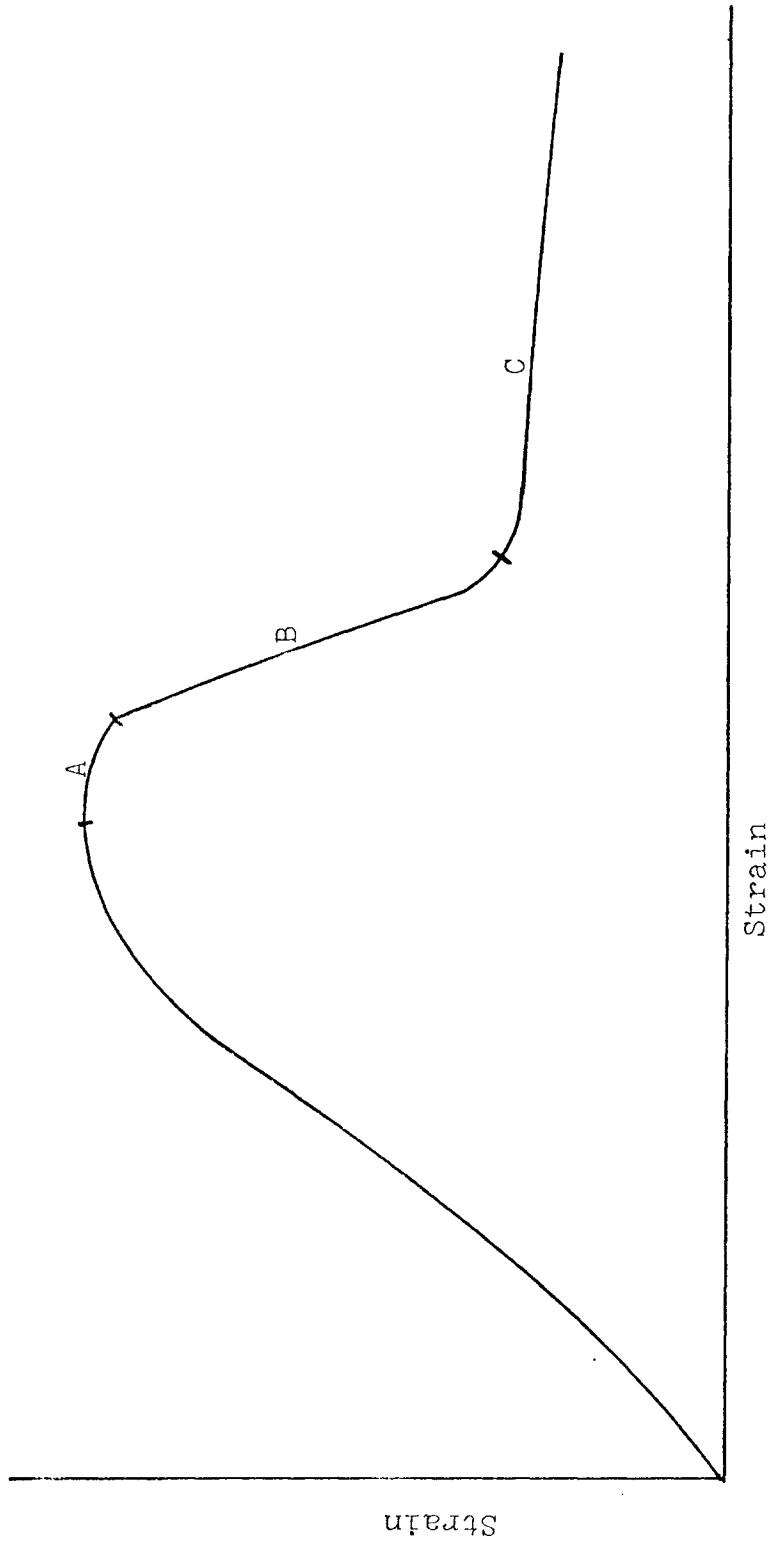


Figure 6. Typical regions of the stress-strain curve in the post-failure zone for the rocks tested in these experiments.

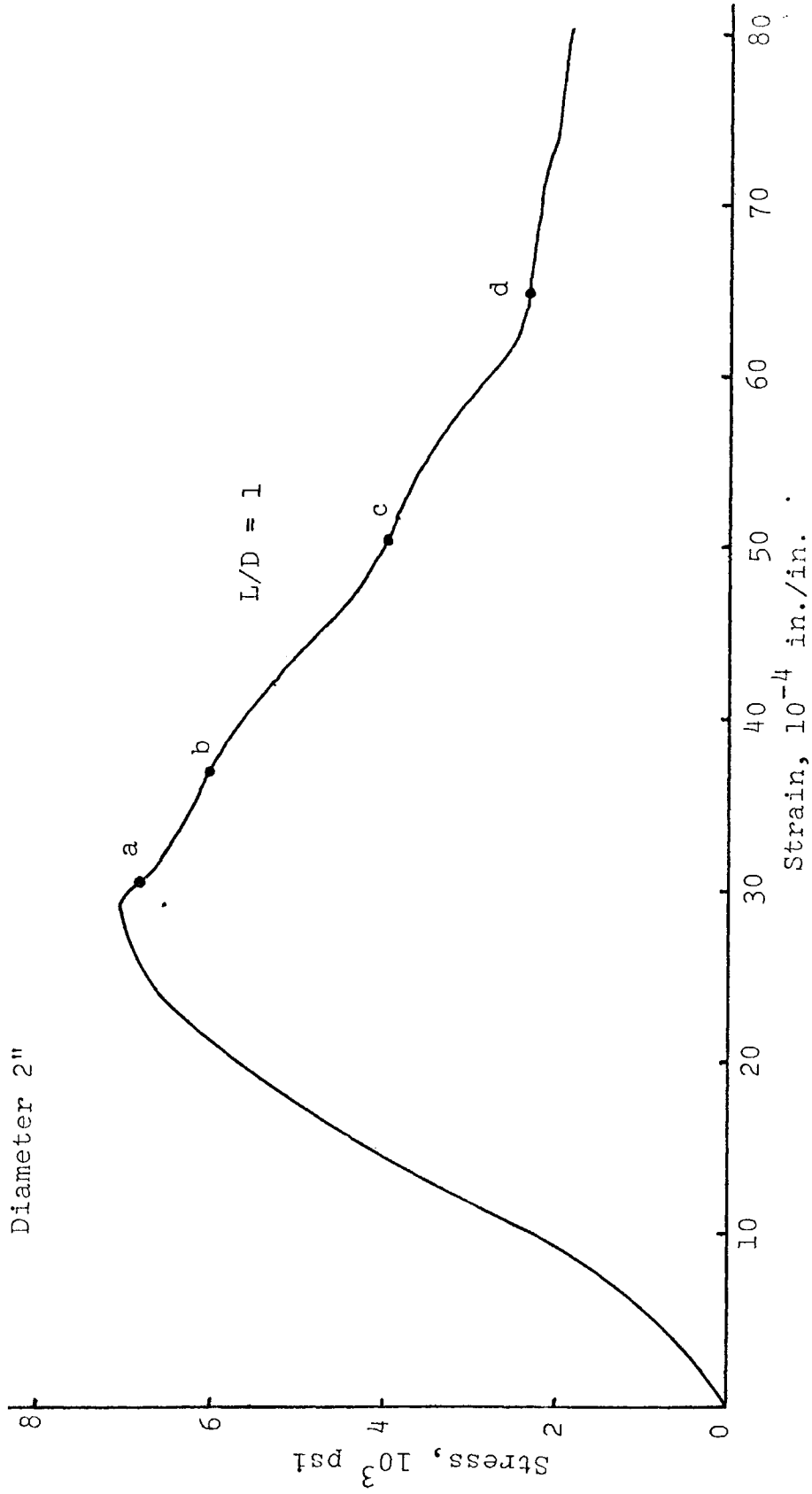
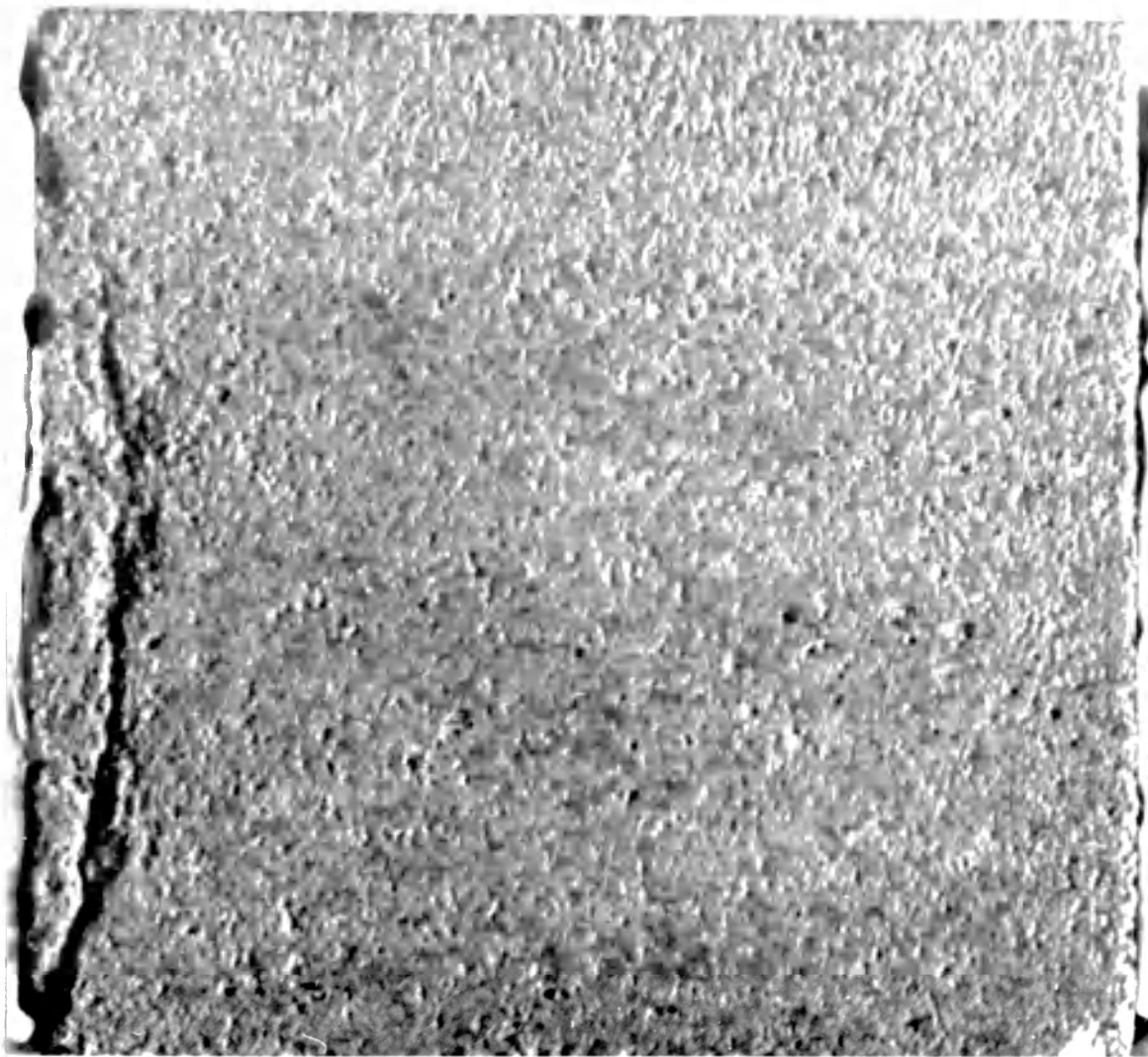
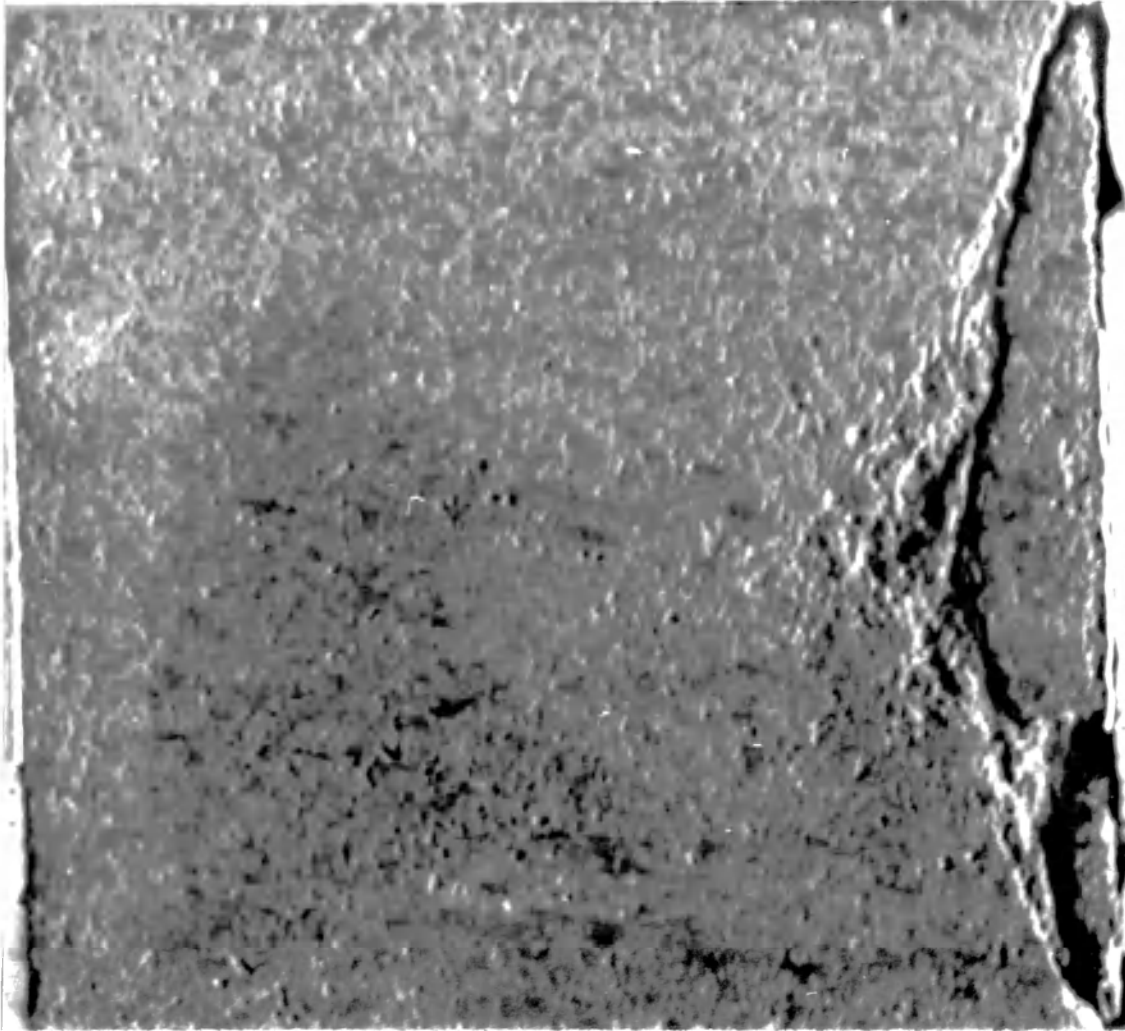


Figure 7. Complete stress-strain curve for Indiana Limestone in uniaxial compression.

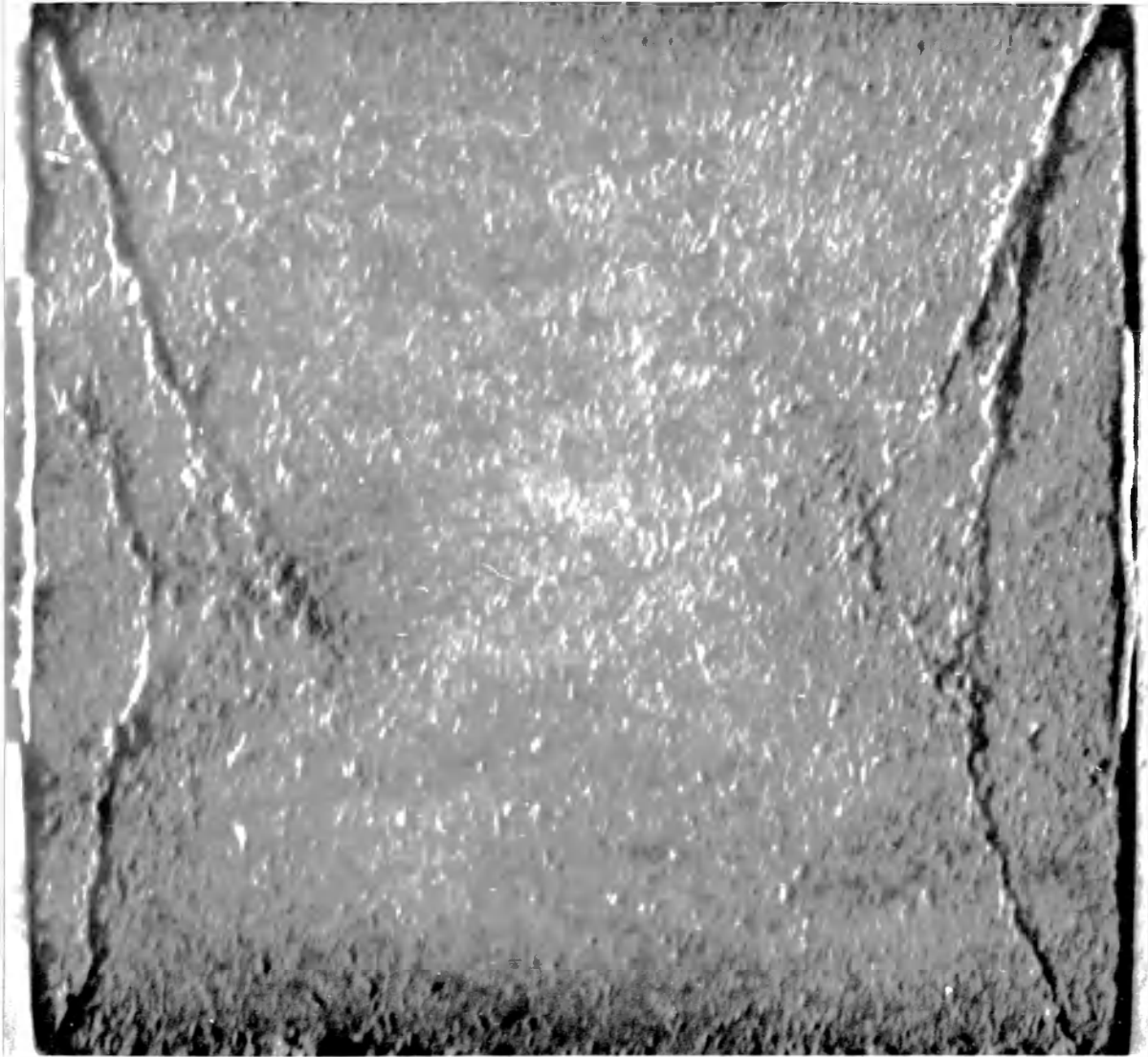


(a)

Figure 8 (a) to (d). Polished sections of Indiana Limestone showing state of failure with increased uniaxial loading along the stress-strain curve. The stress-strain curve is shown in Figure 7.



8 (b)



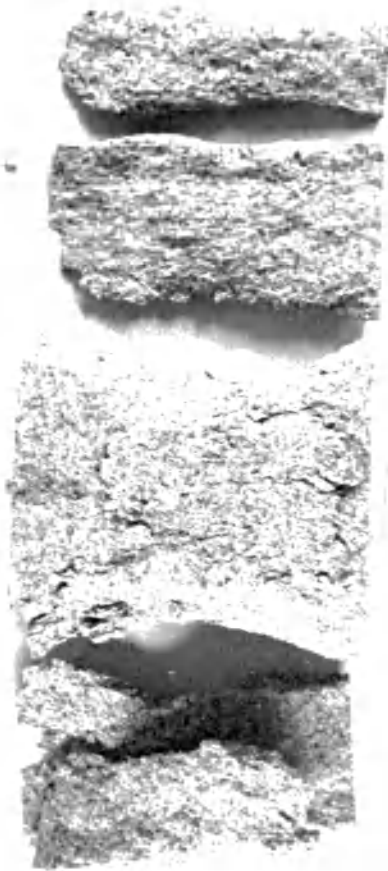
8 (c)



8 (a)



(b) Diameter 1.25", Length 2.25"
(L/D = 1.5)



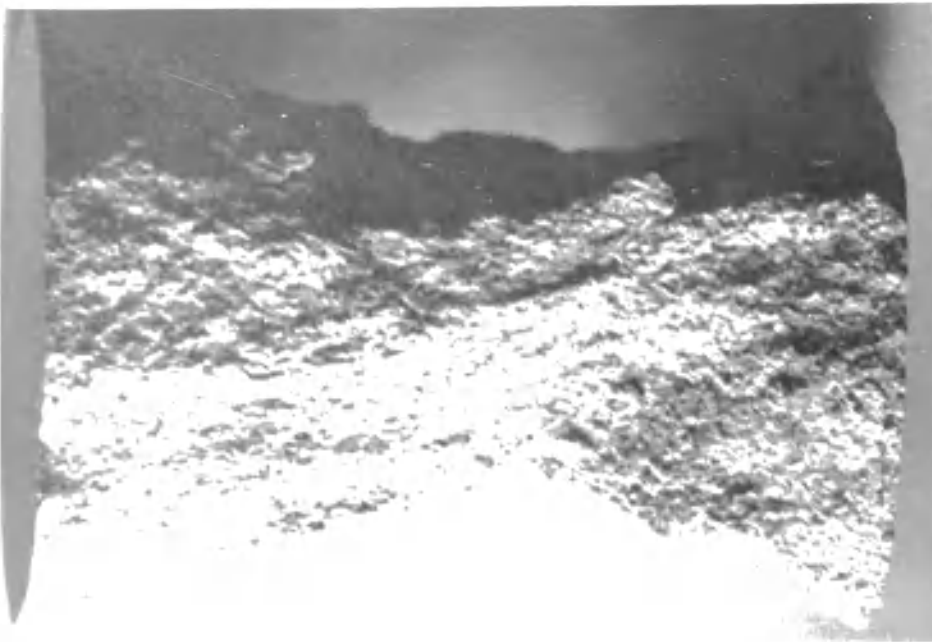
LIMESTONE 2" x 2"

(a) Diameter 2", Length 2"
(L/D = 1.0)

Figure 9 (a) to (d). Unconfined Indiana Limestone in advanced stages of failure. Two different shapes and two different size specimens are shown.



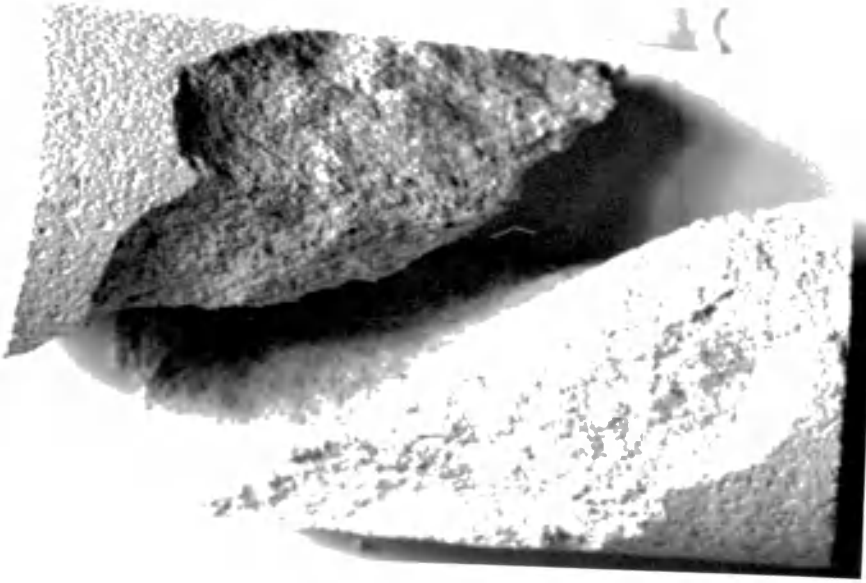
(d) Diameter 2.0", Length 3"
(L/D = 1.5)



(c) Diameter 1.5", Length 1.5"
(L/D = 1)

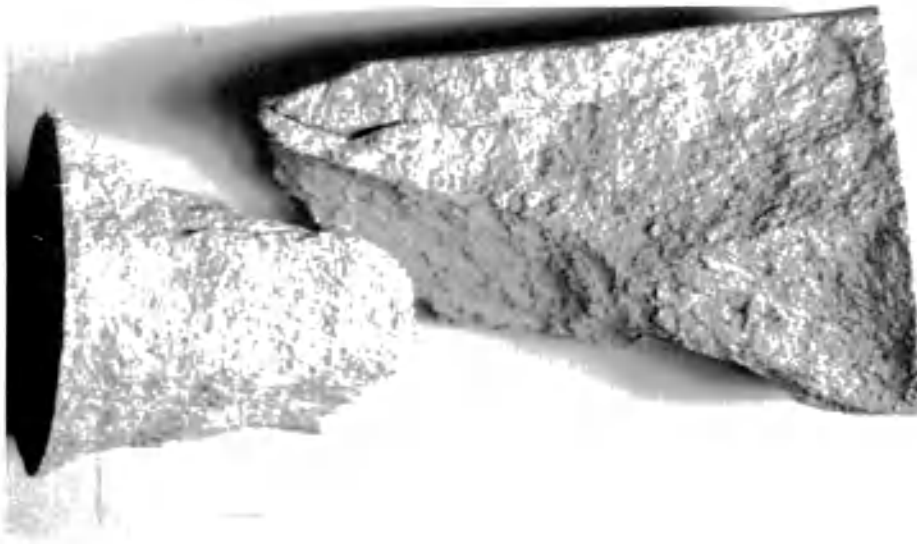


(a) Diameter 2", Length 4"
(L/D = 2)



(b) Diameter 1.5", Length 3.0"
(L/D = 2.0)

Figure 10 (a) and (b). Complete failed samples of Indiana Limestone tested in uniaxial compression.



Diameter 2", Length 3"

Figure 12. Typical failure mode of unconfined Indiana Limestone loaded in a conventional testing machine.

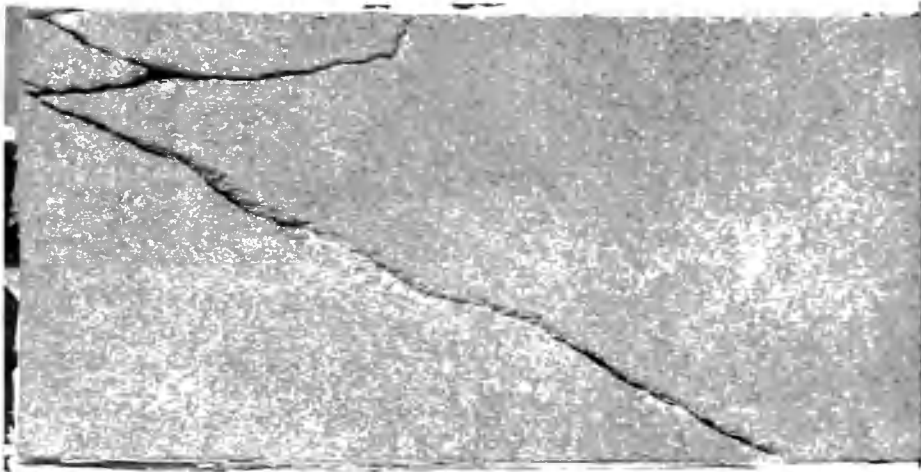
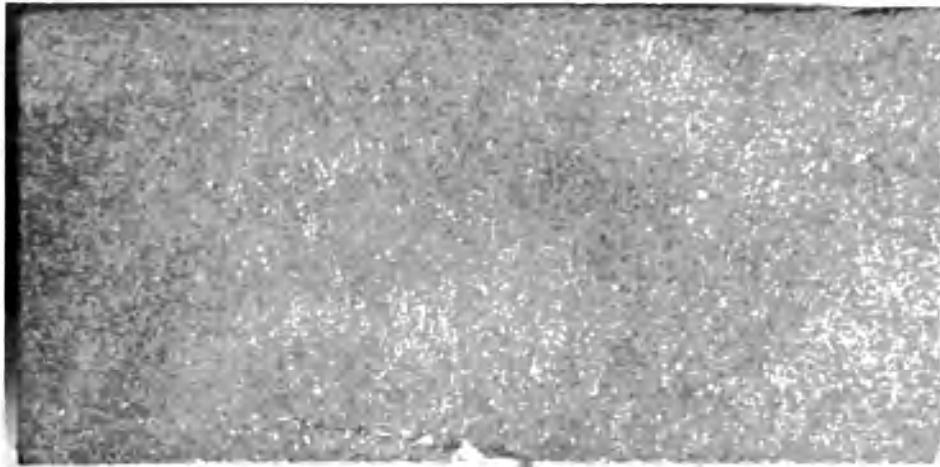


Figure 11. Sample sections of partially failed Indiana Limestone in uniaxial compression.

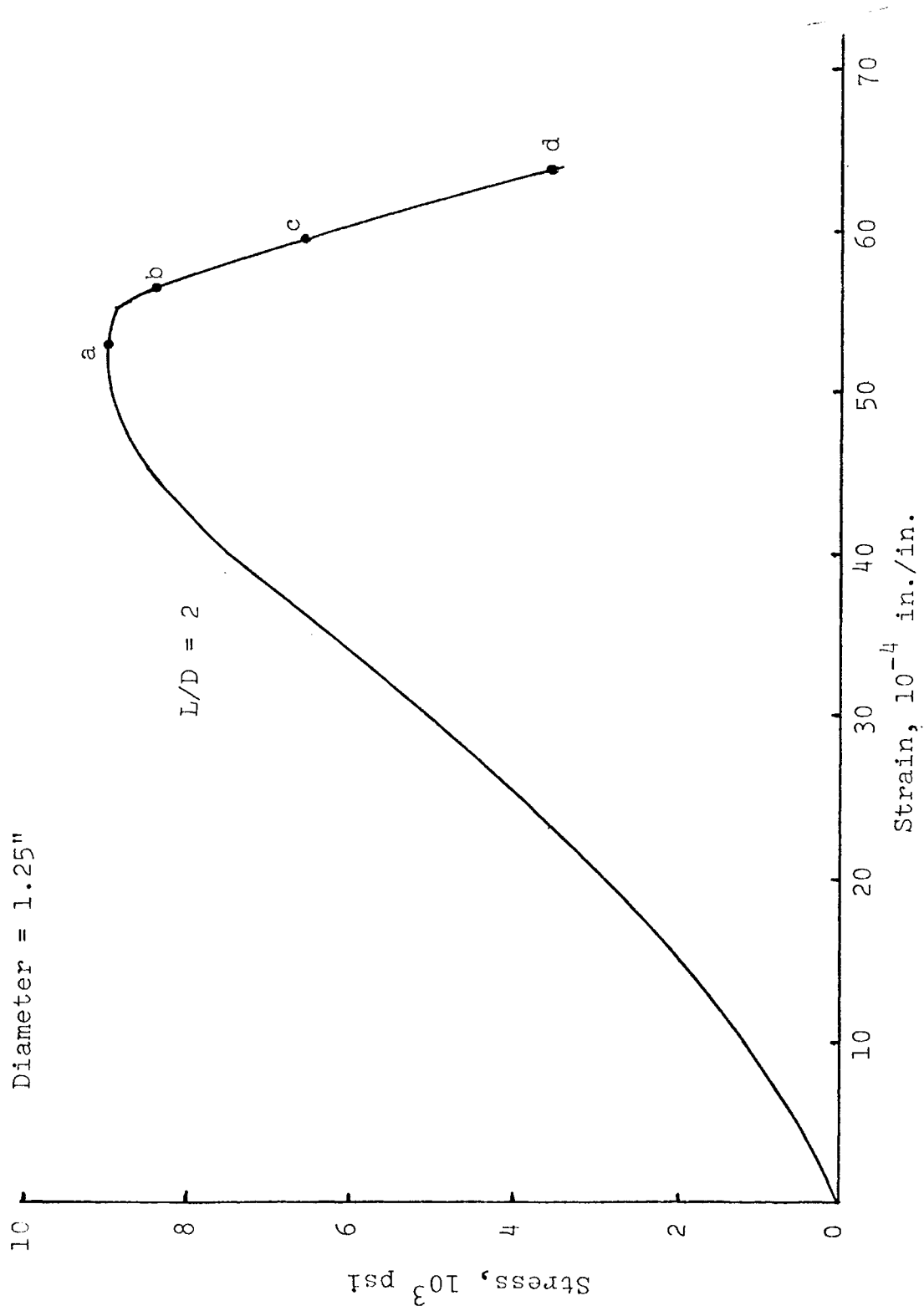
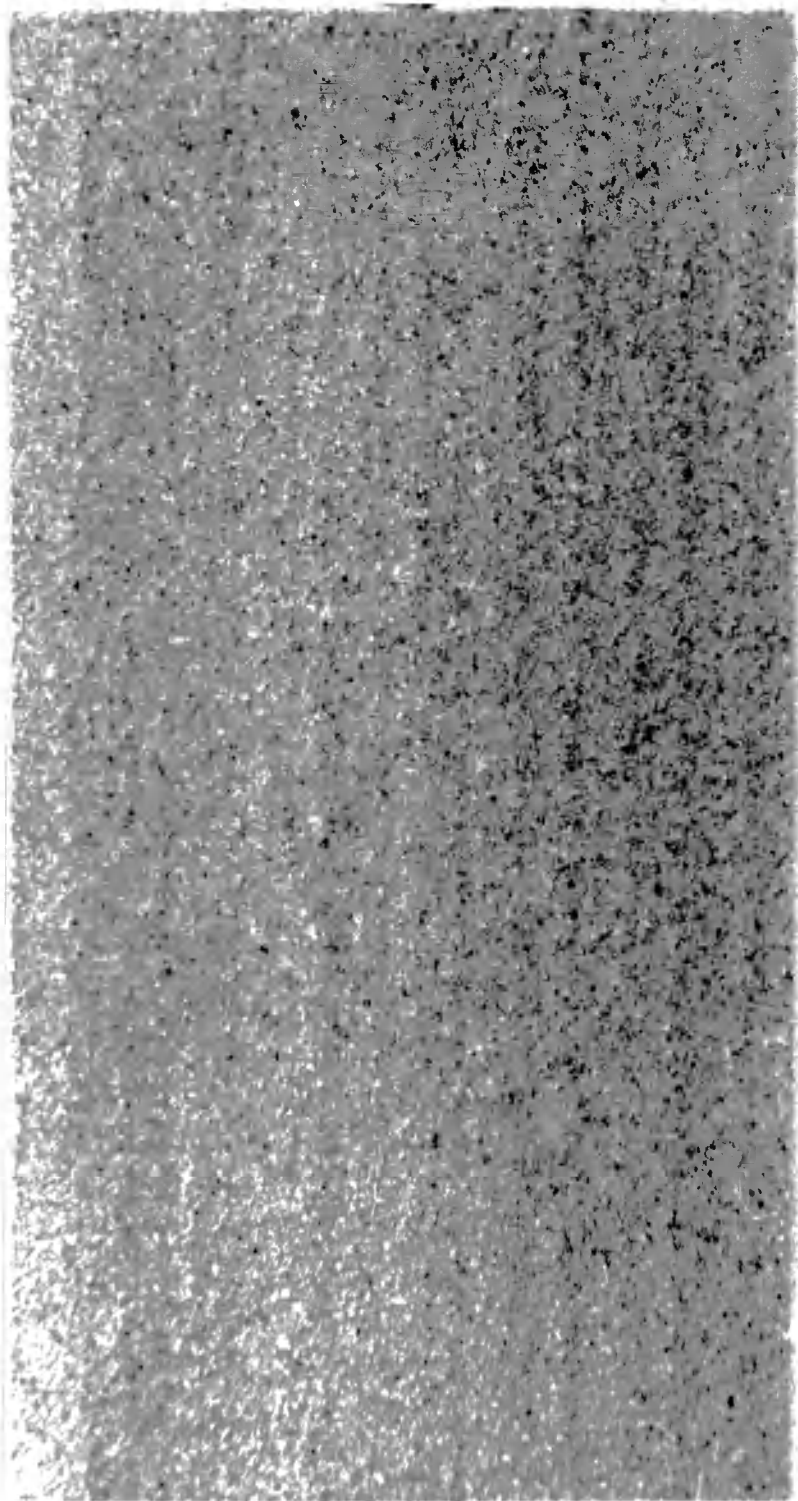


Figure 13. Complete stress-strain curve for sandstone in uniaxial compression.



(a)

Figure 14 (a) to (d). Polished sections of sandstone showing state of failure with increased uniaxial loading along the stress-strain curve. The stress-strain curve is shown in Figure 13.



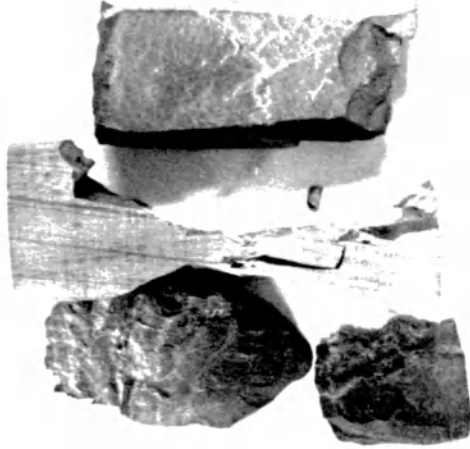
14 (b)

14 (b)





14 (d)



(b) Diameter = 0.825"
 Length = 2.0"
 (L/D = 2.5)



(a) Diameter = 0.825"
 Length = 2.47"
 (L/D = 3.0)

Figure 15 (a) and (b). Remnants of oil shale samples loaded in uniaxial compression.

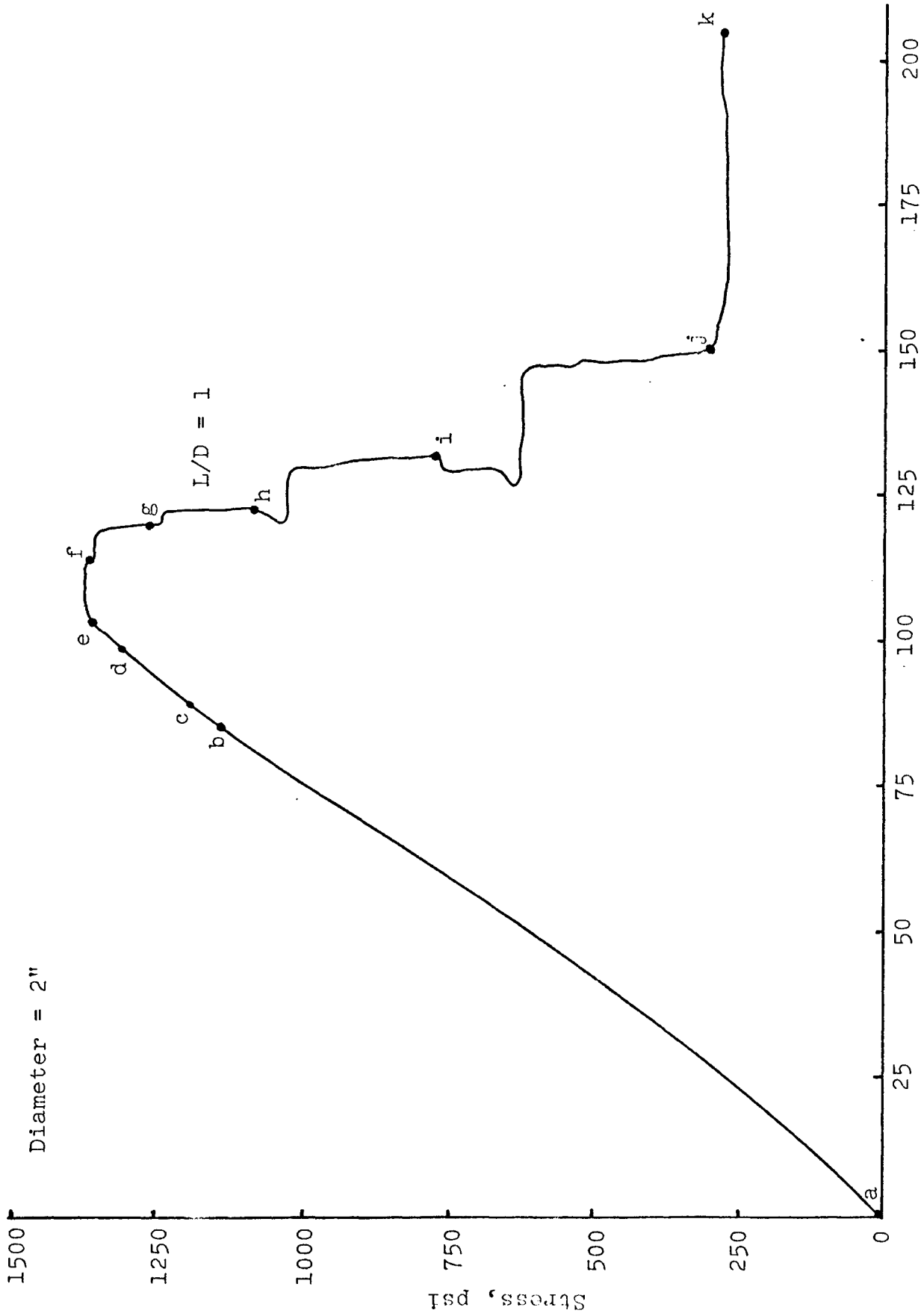


Figure 16. Complete stress-strain curve for coal in uniaxial compression.



(a)

Figure 17 (a) to (k). Series of photographs taken at various points along the stress-strain curve for a coal sample tested in uniaxial compression. The stress-strain curve is shown in Figure 16.



(b)



(c)



(d)



(e)



(f)



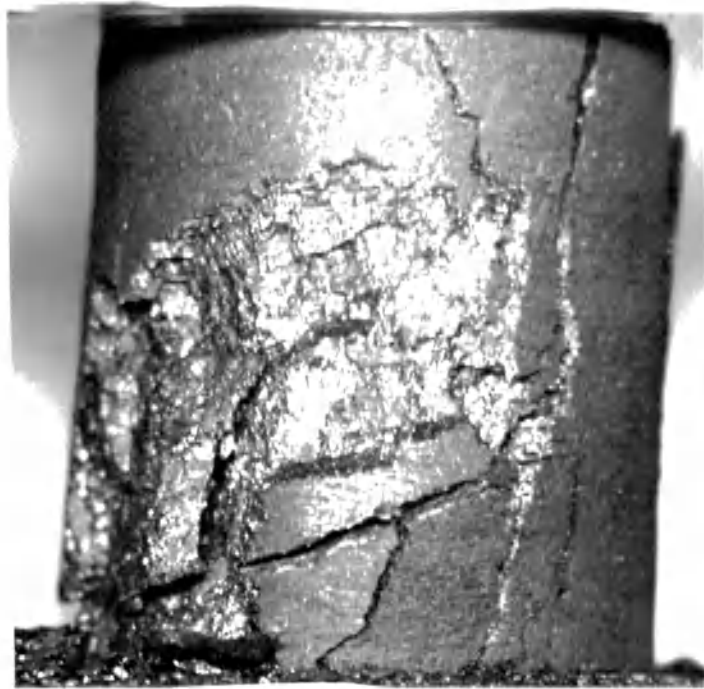
(g)



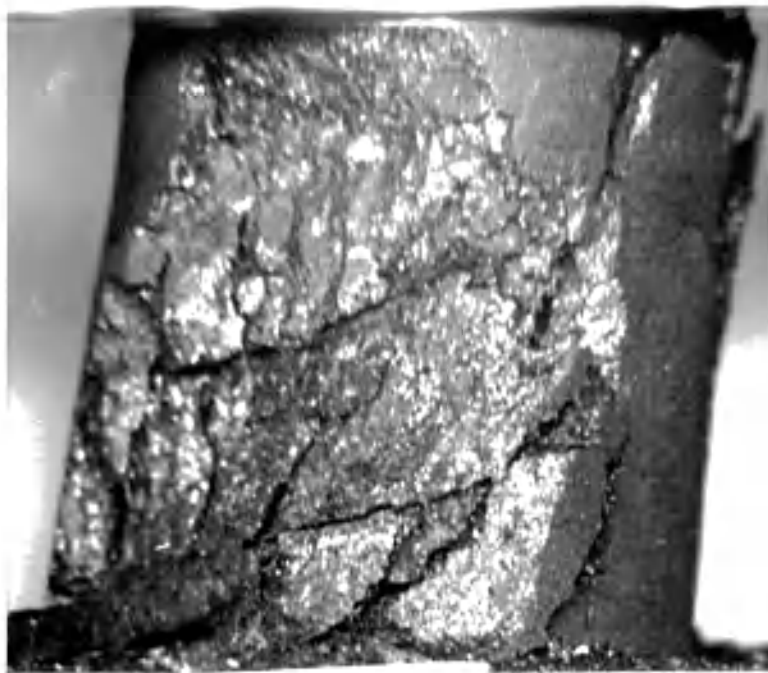
(h)



(i)



(j)



(k)

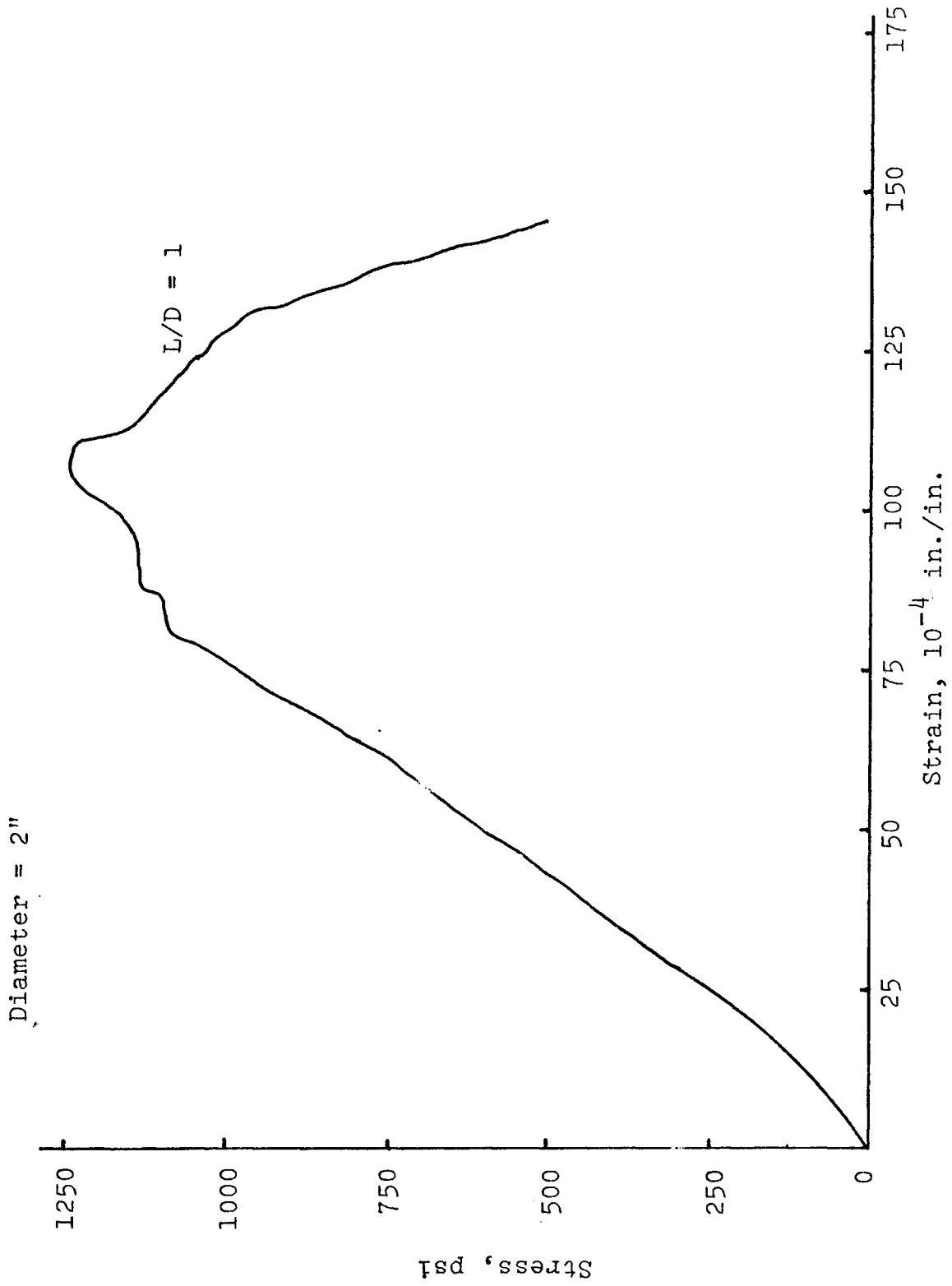


Figure 18. Complete stress-strain curve for coal in uniaxial compression.

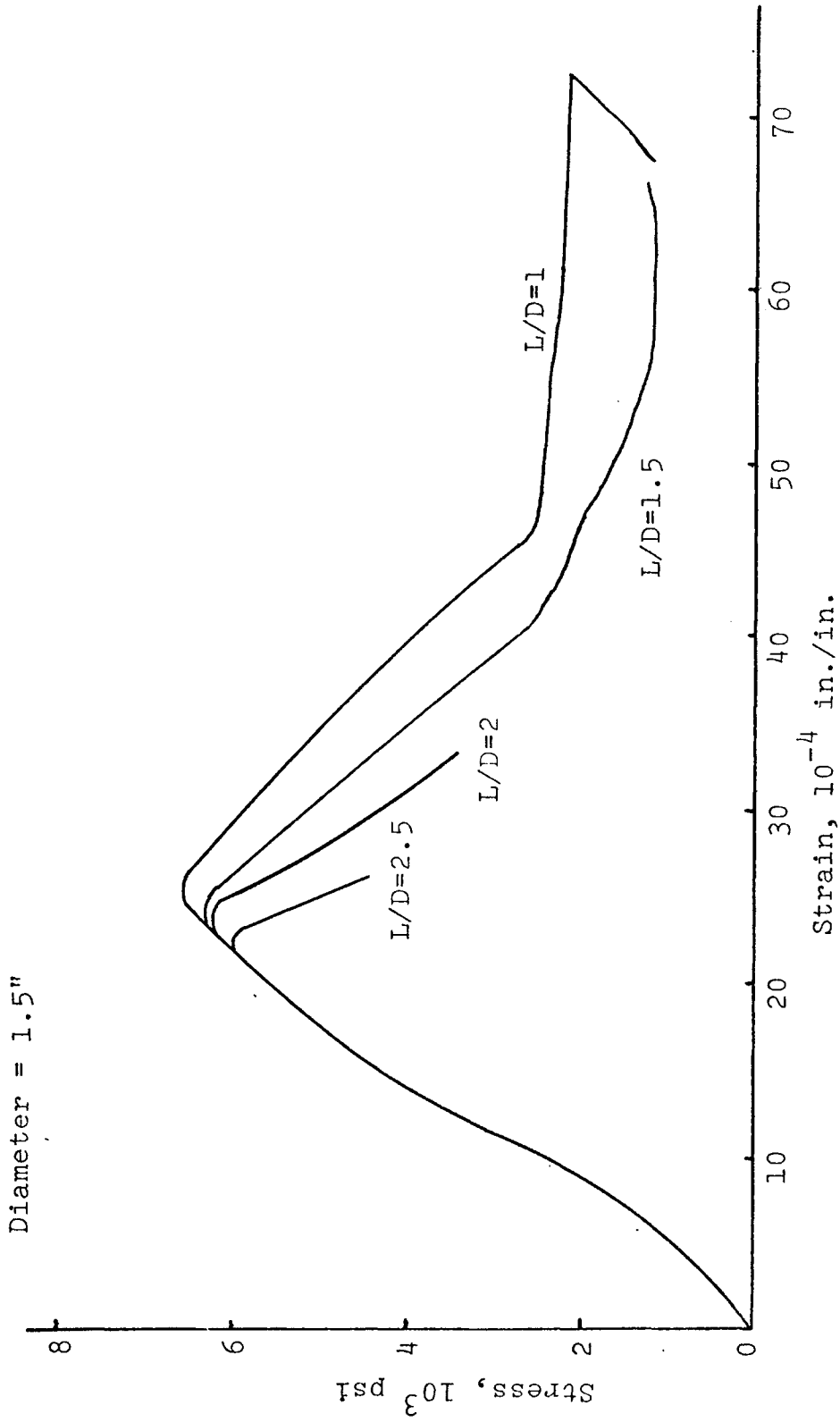


Figure 19. Influence of specimen shape on the complete stress-strain curve for Indiana Limestone in uniaxial compression.

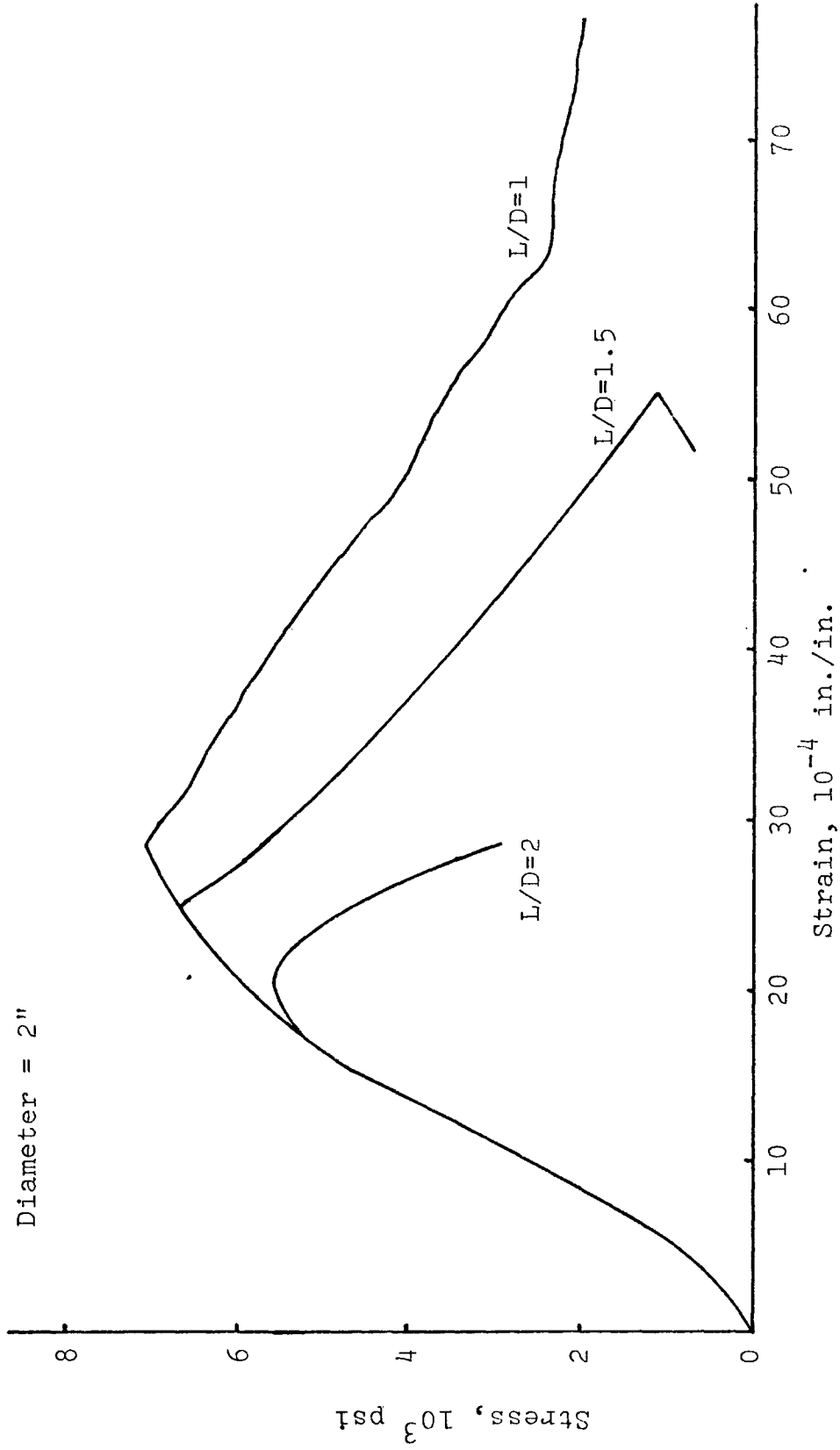


Figure 20. Influence of specimen shape on the complete stress-strain curve for Indiana Limestone in uniaxial compression.

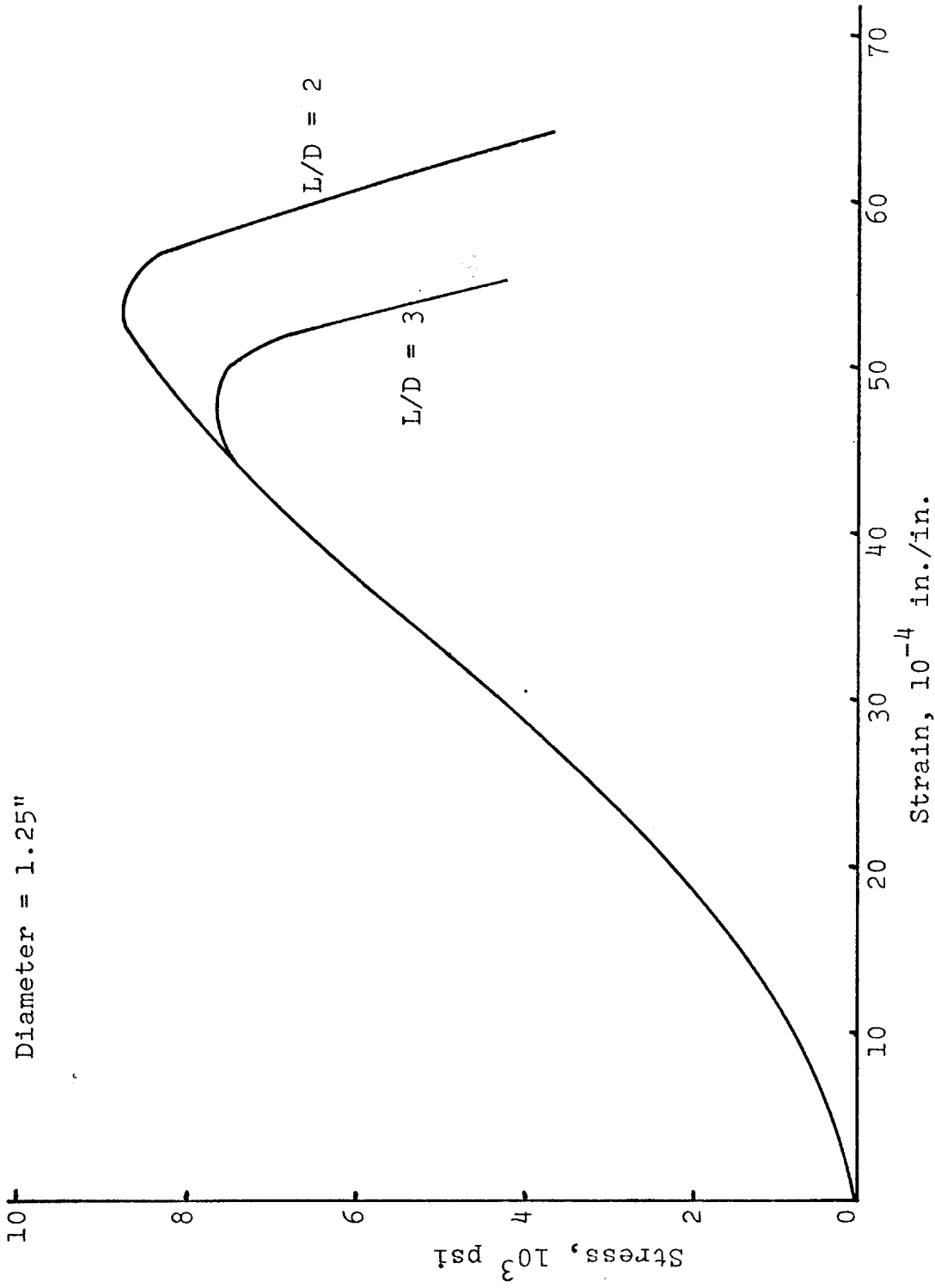


Figure 21. Influence of specimen shape on the complete stress-strain curve for sandstone in uniaxial compression.

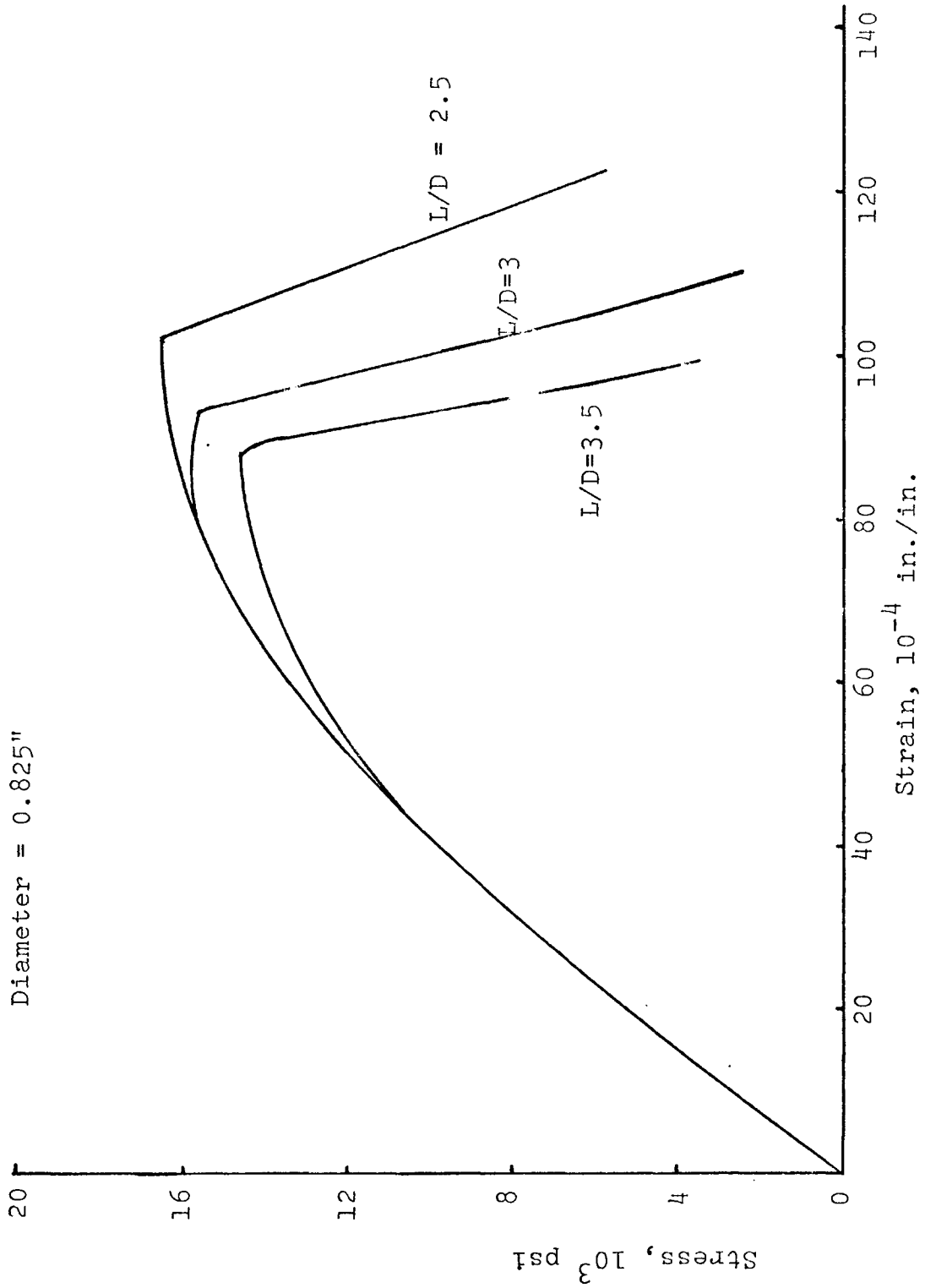


Figure 22. Influence of specimen shape on the complete stress-strain curve for oil shale in uniaxial compression.

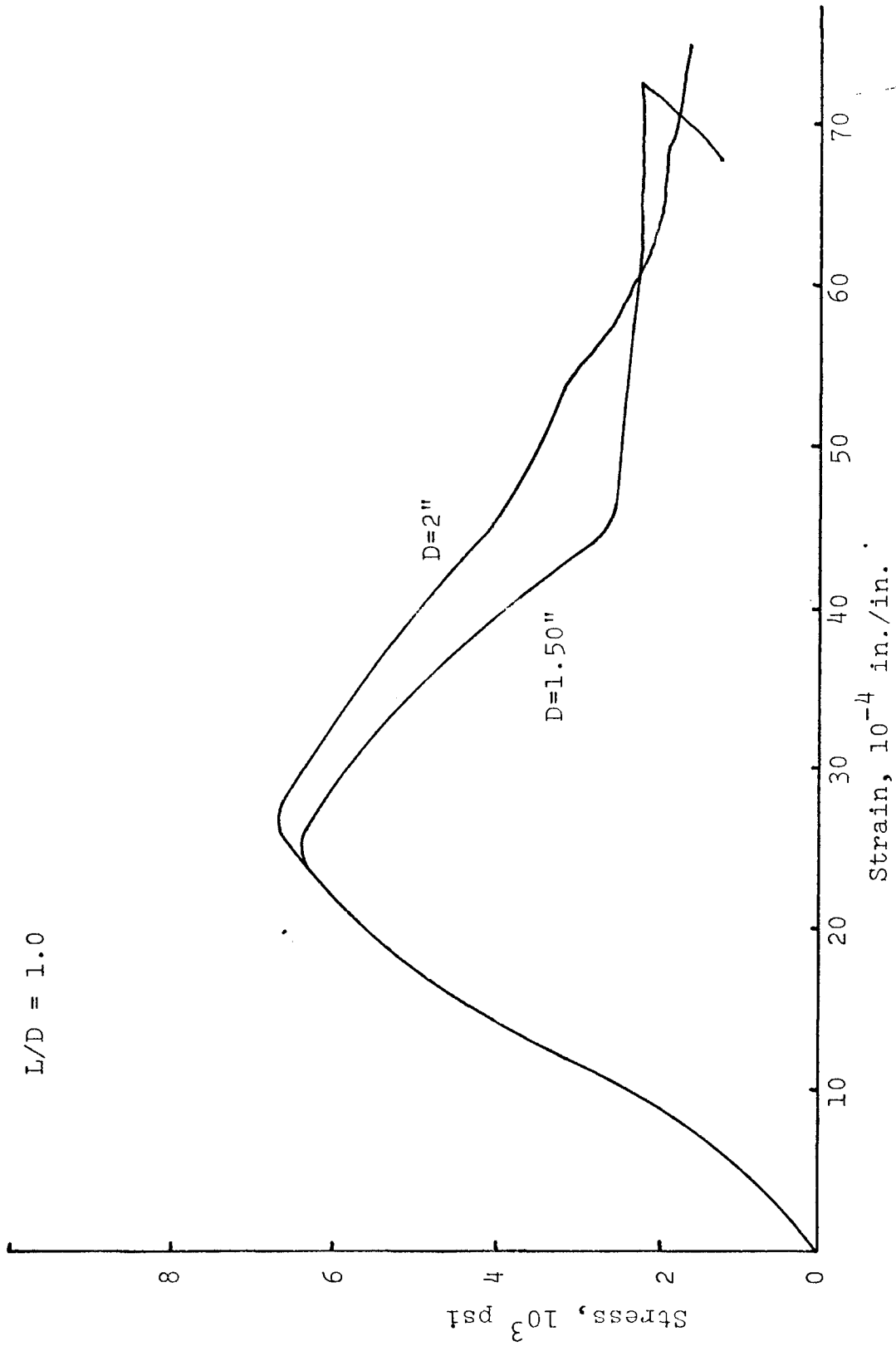


Figure 23. Influence of specimen size on the complete stress-strain curve for Indiana Limestone in uniaxial compression.

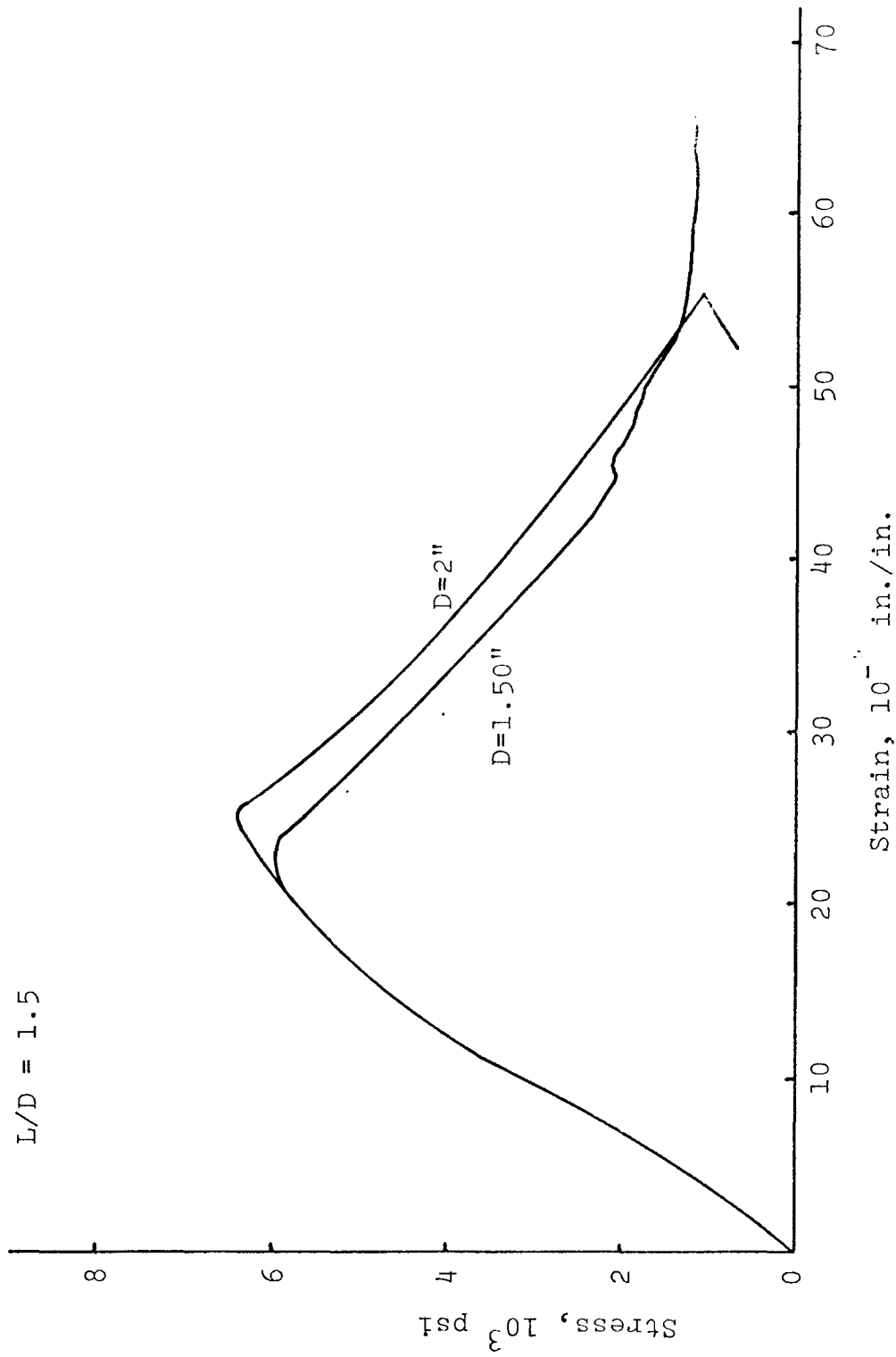


Figure 24. Influence of specimen size on the complete stress-strain curve for Indiana Limestone in uniaxial compression.

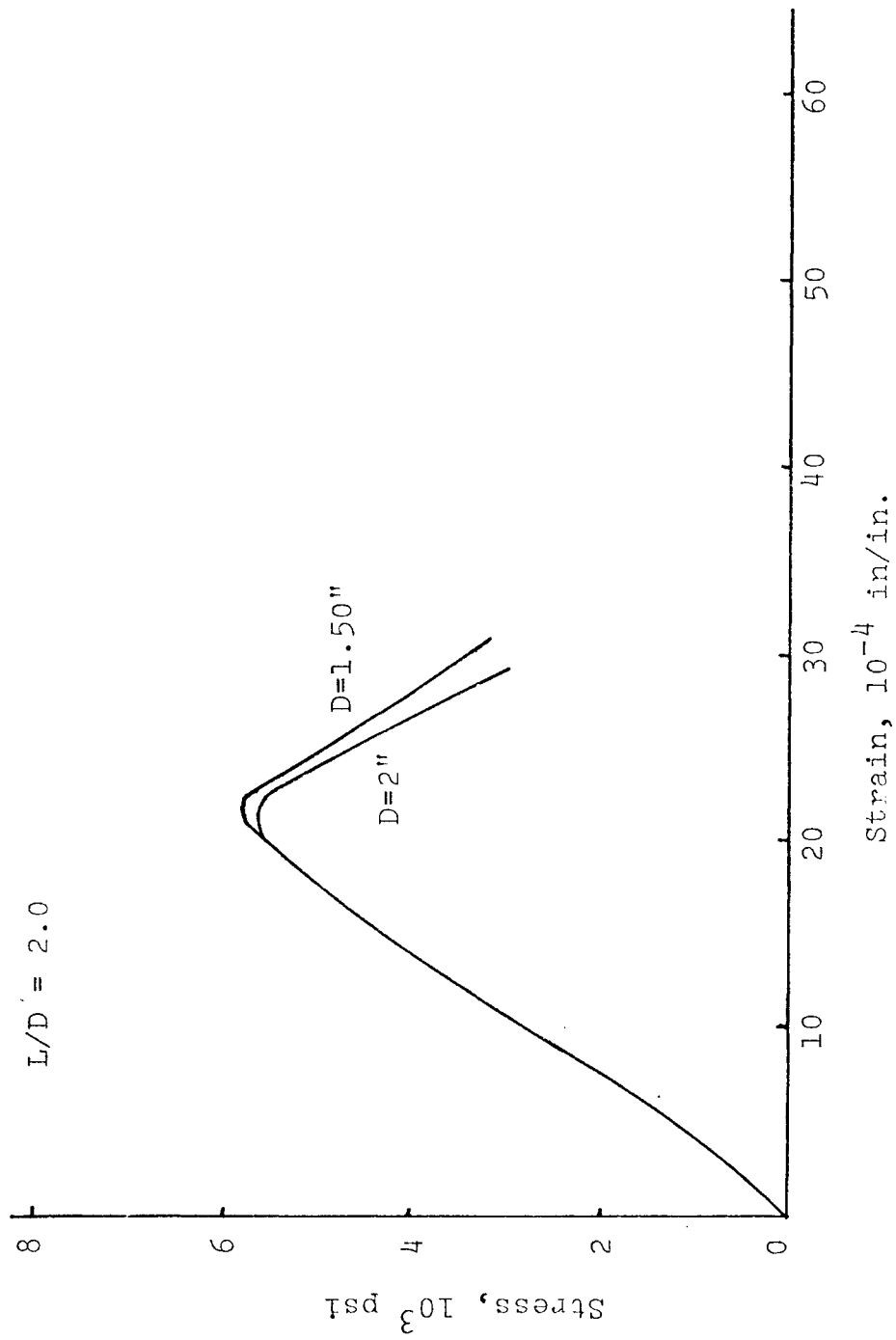


Figure 25. Influence of specimen size on the complete stress-strain curve for Indiana Limestone in uniaxial compression.

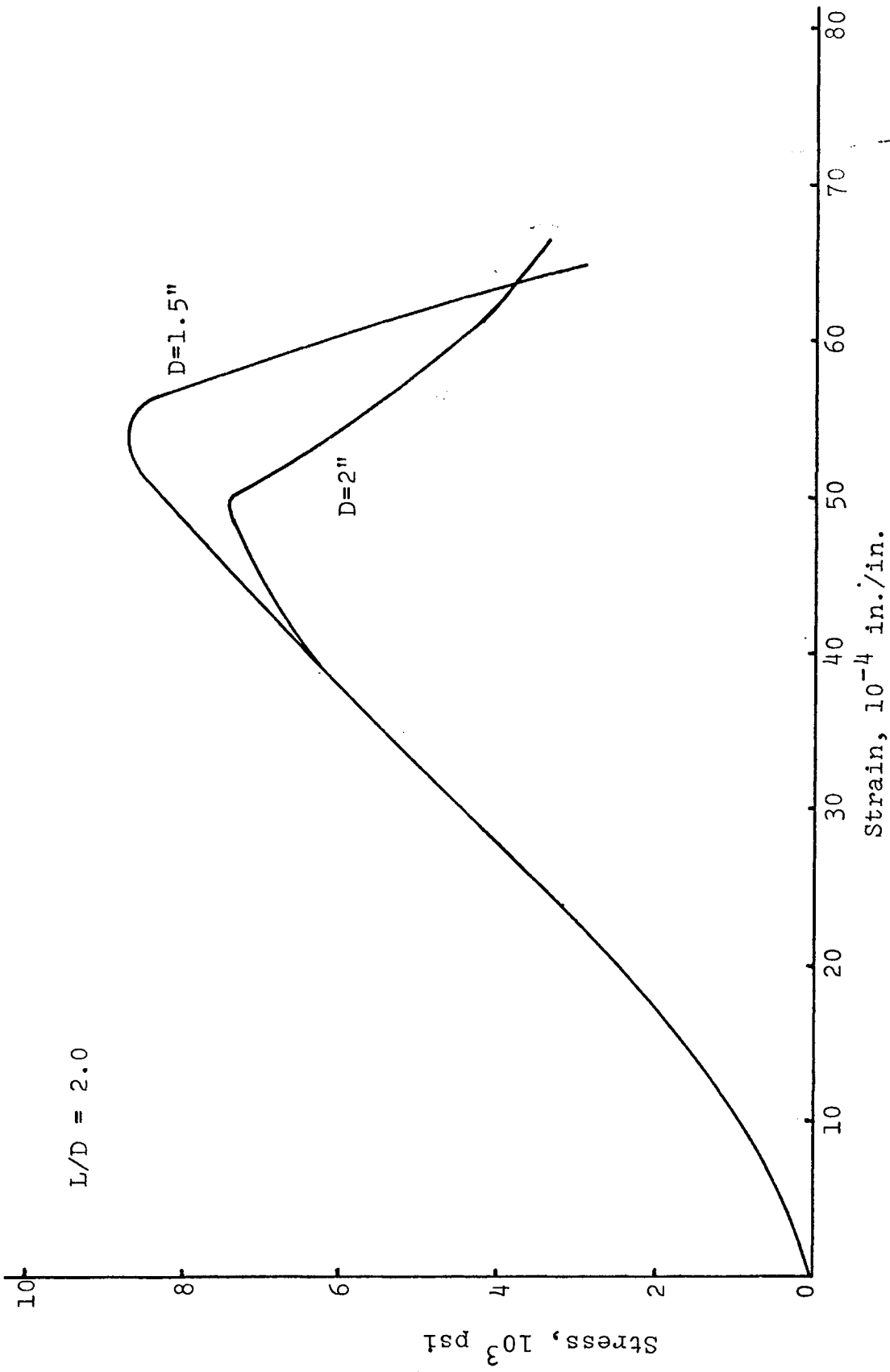


Figure 26. Influence of specimen size on the complete stress-strain curve for sandstone in uniaxial compression.

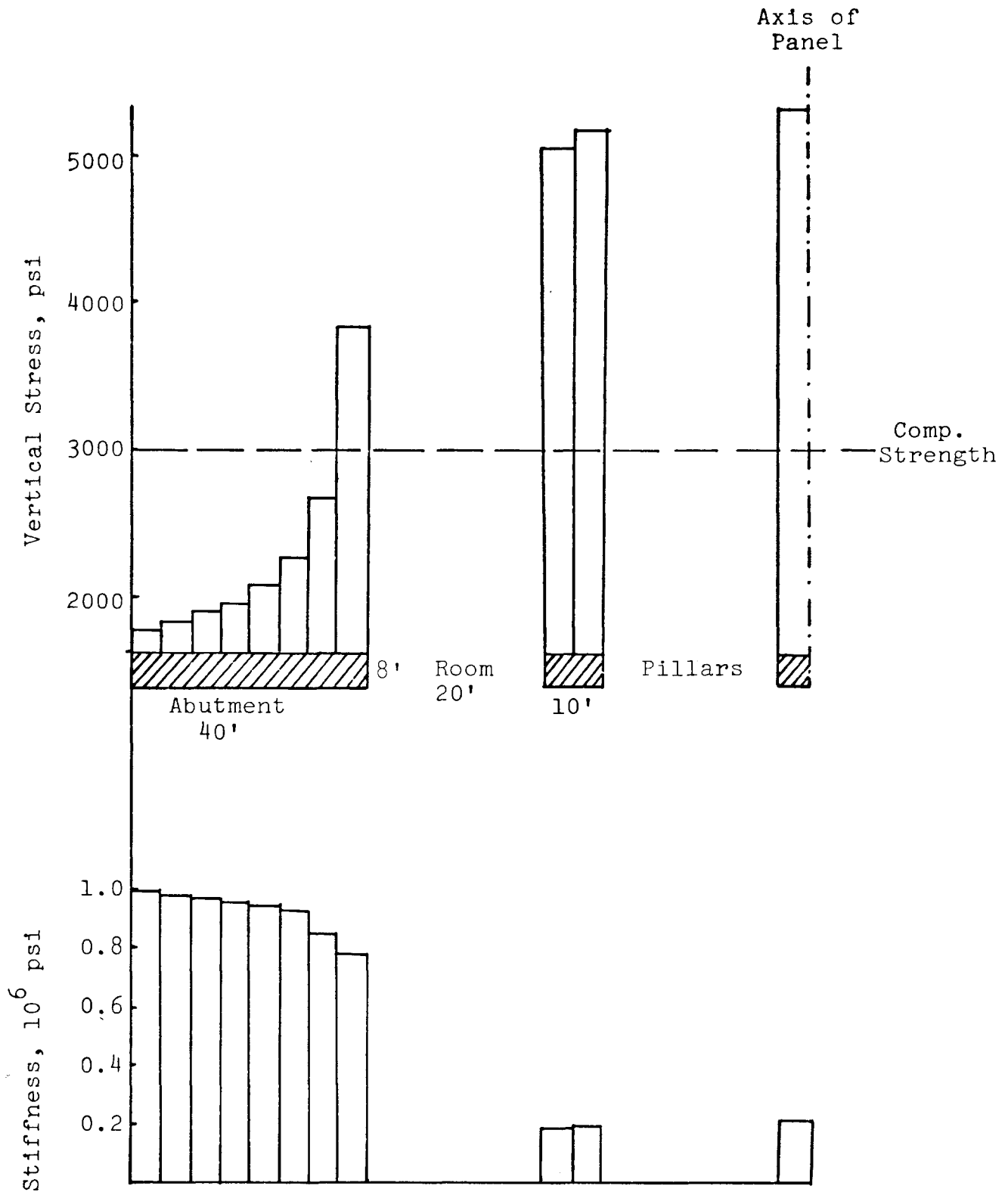


Figure 27. Distribution of stresses and stiffnesses for a four-room panel.

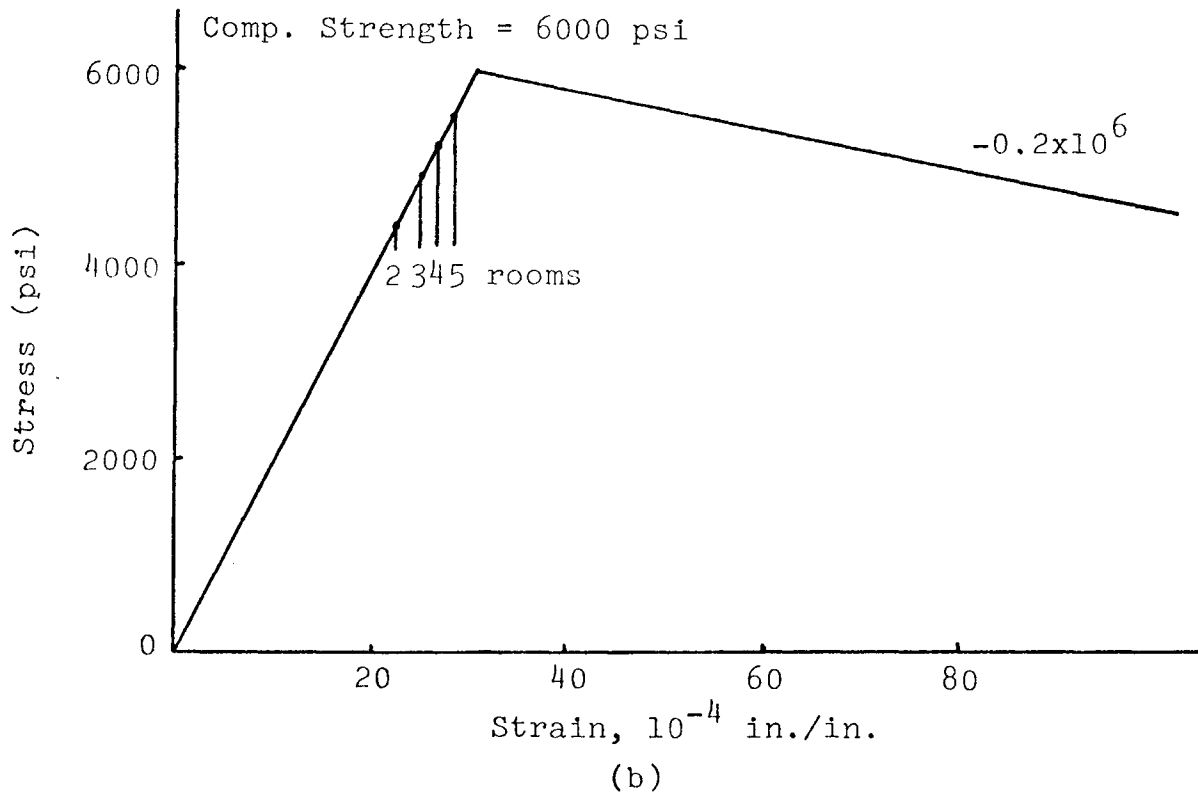
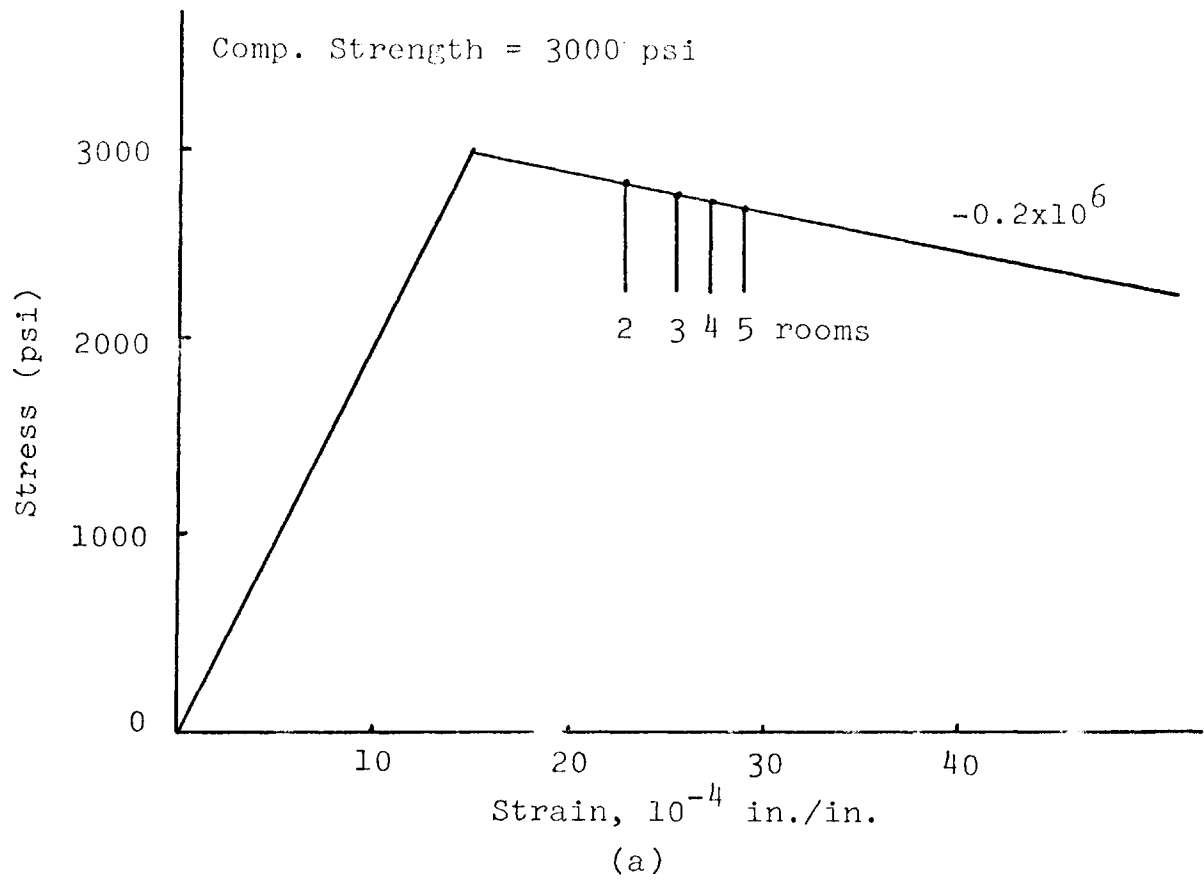
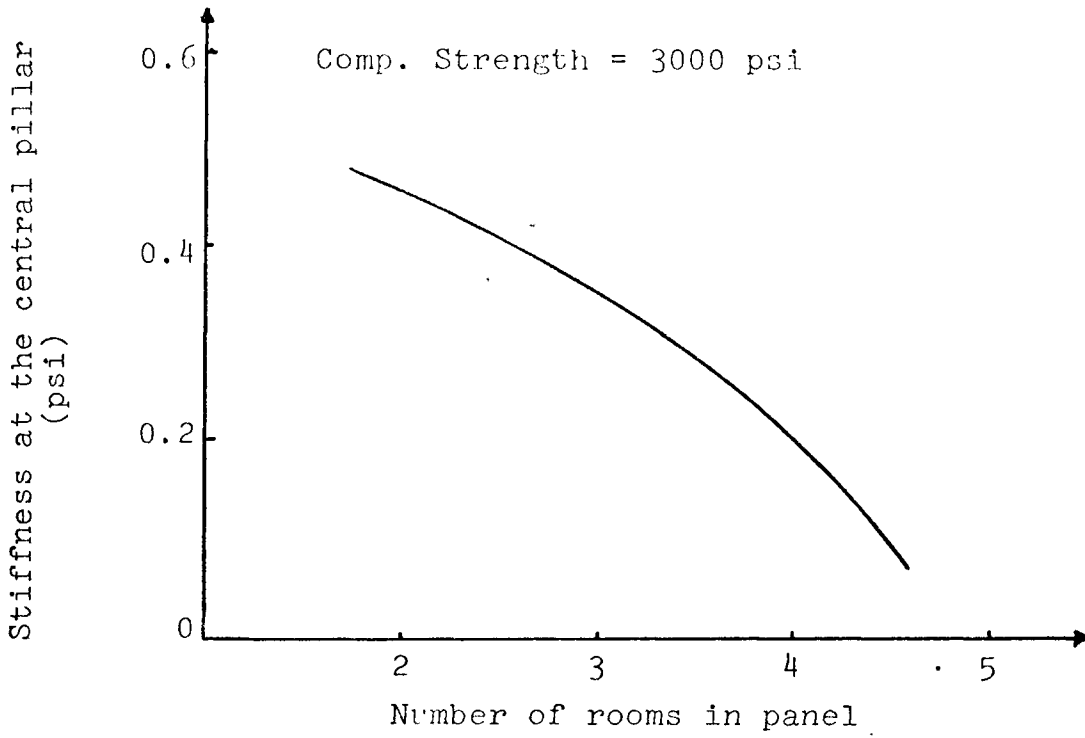
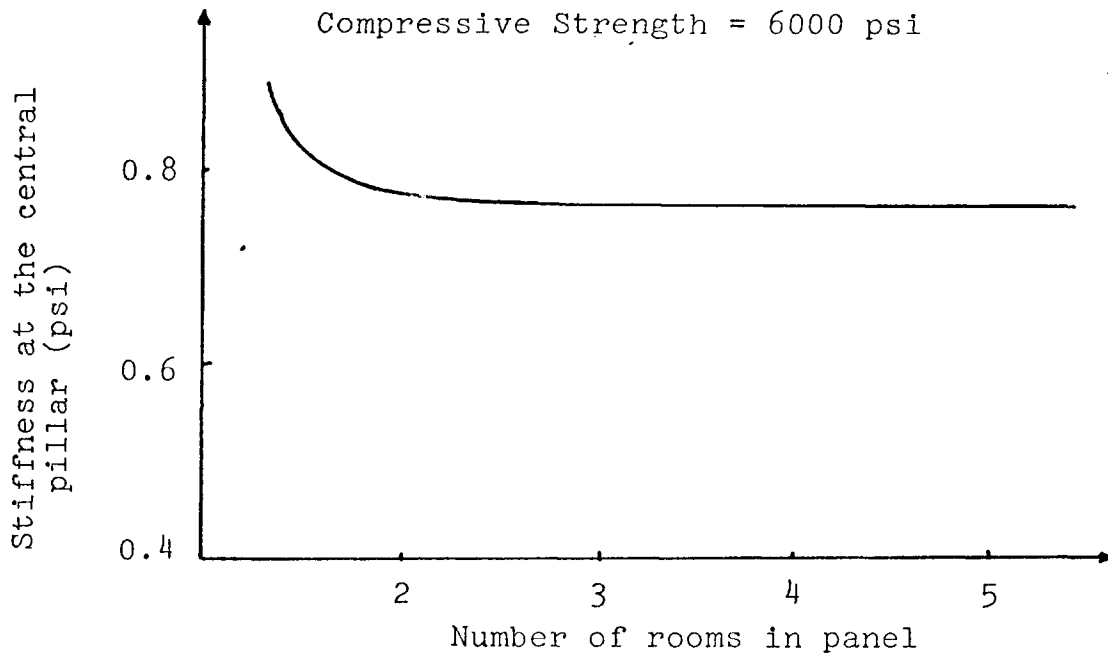


Figure 28. State of stress in the central pillar as mining progresses.



(a)



(b)

Figure 29. Variation of the stiffness at the central pillar as mining progresses.

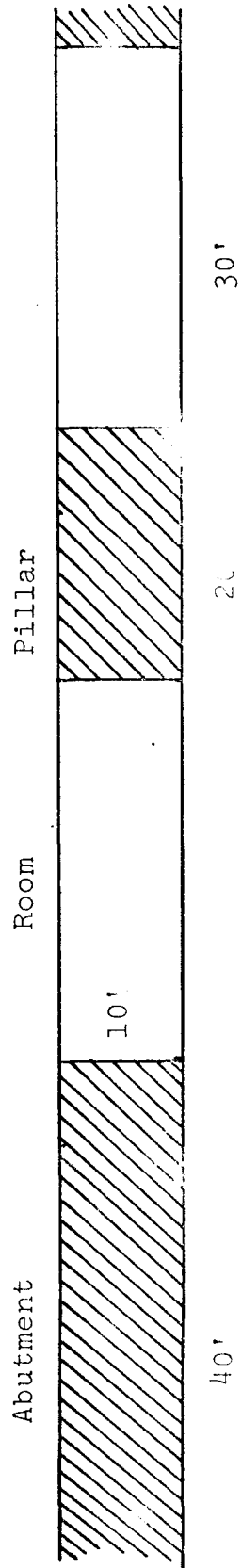


Figure 30. Layout of the excavation for the second example.

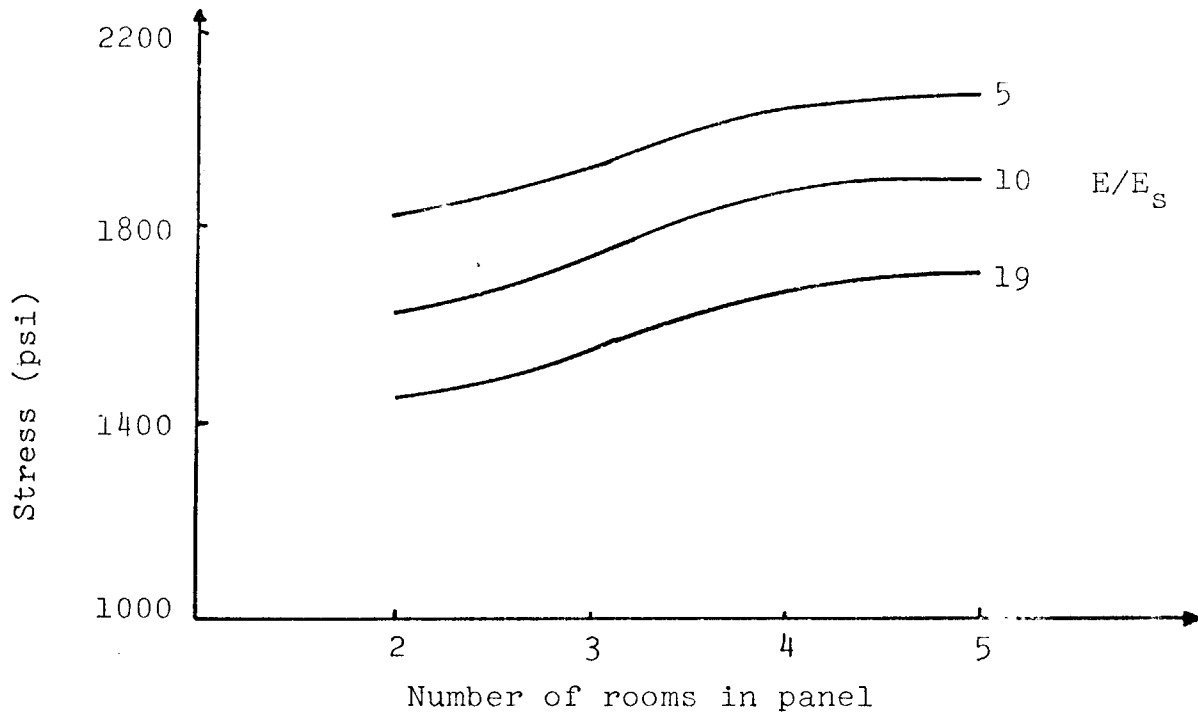


Figure 31. Variation of stresses with the value of E/E_s .

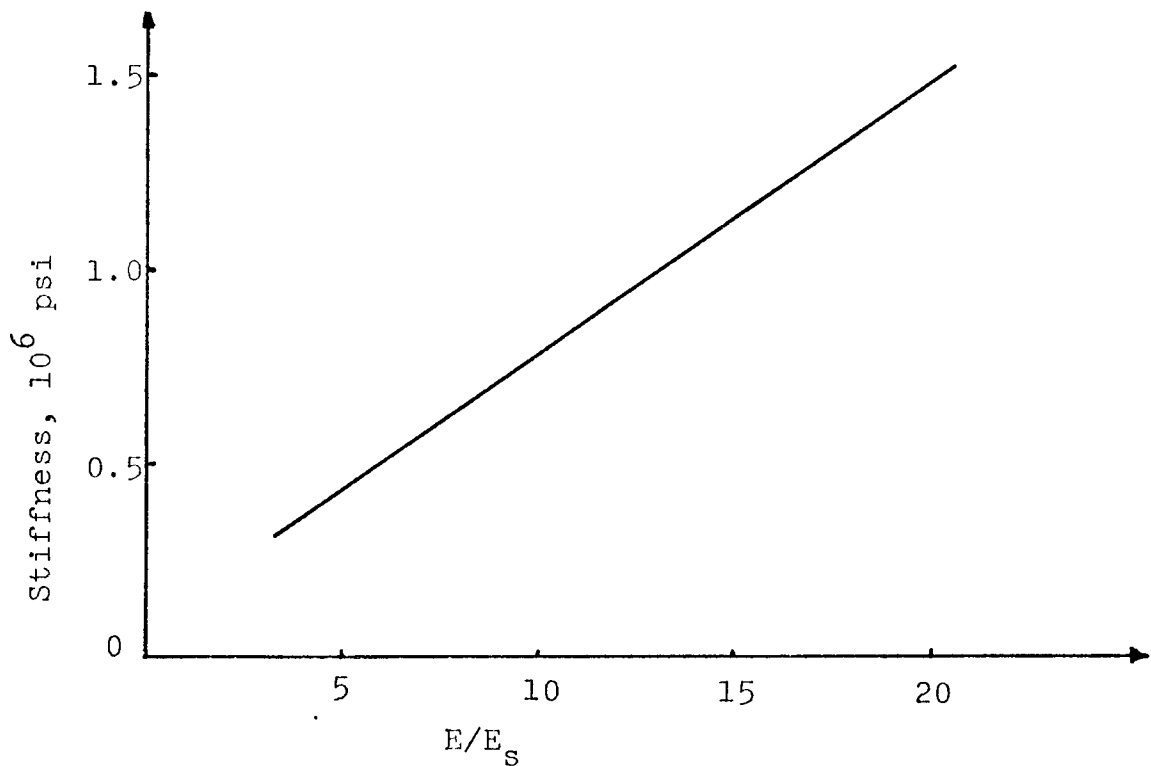


Figure 32. Variation of the stiffness with the value of E/E_s for a two-room panel.

APPENDIX A
DETERMINATION OF THE SAMPLE DEFORMATION

The deformation measured using the DCDTs consists of contributions from both the sample being tested and from the steel platens. One must separate these deformations so that the sample strain can be calculated. The length of platen involved can be determined with the analyses and calibration procedure described below. Once this length has been found, the platen deformation for any particular stress level can be calculated and subtracted from the total deformation to give the sample deformation.

Assume the following sample, platen deformation occurs under a stress σ .

Δl_s = shortening of sample

Δl_p = shortening of platen.

The total deformation (Δl) is given by (measured)

$$\Delta l = \Delta l_s + \Delta l_p \quad (1)$$

Neglecting the effect of platen shortening, the apparent elastic modulus (E_m) of the sample in the machine would be

$$E_m = \frac{\sigma}{\frac{\Delta l_s + \Delta l_p}{l_s}} = \frac{\sigma}{\frac{\Delta l_s}{l_s} + \frac{\Delta l_p}{l_s}} \quad (2)$$

where

E_m = apparent elastic modulus

l_s = length of the sample.

However, the true elastic modulus (E_s) is

$$E_s = \frac{\sigma}{\frac{\Delta l_s}{l_s}} \quad (3)$$

and neglecting the platen contribution can result in serious errors. Letting

$$\Delta l_s = \epsilon_s l_s = \frac{\sigma_s}{E_s} l_s \quad (4)$$

$$\Delta l_p = \epsilon_p l_p = \frac{\sigma_p}{E_p} l_p \quad (5)$$

where

ϵ_s = strain in sample under stress σ_s

ϵ_p = strain in platens under stress σ_p

E_s = elastic modulus of sample

E_p = elastic modulus of the platen.

For $\sigma_s = \sigma_p$, then

$$\frac{\Delta l_p}{\Delta l_s} = \frac{E_s}{E_p} \frac{l_p}{l_s} \quad (6)$$

Letting

$$l_p = A l_s \quad (7)$$

where: A = constant.

Then,

$$\frac{\Delta l_p}{\Delta l_s} = \frac{E_s}{E_p} A \quad (8)$$

Dividing both sides by l_s and rearranging, one finds that

$$\frac{\Delta l_p}{l_s} = \frac{E_s}{E_p} A \frac{\Delta l_s}{l_s} \quad (9)$$

Substituting equation (9) into equation (2) one obtains

$$E_m = \frac{\sigma}{\frac{\Delta l_s}{l_s} (1 + A \frac{E_s}{E_p})} \quad (10)$$

But since

$$\frac{\Delta l_s}{l_s} = \frac{\sigma}{E_s}$$

equation (10) can be written as

$$E_m = \frac{E_s E_p}{E_p + A E_s} \quad (11)$$

Solving equation (12) for A and E_s one finds, respectively

$$A = E_p \left[\frac{E_s - E_m}{E_m E_s} \right] \quad (12)$$

$$E_s = \frac{E_m E_p}{E_p - A E_m} \quad (13)$$

The value of A was obtained experimentally in the following manner. A steel cylinder 2 inches in diameter and 4 inches in length having a known (measured using strain gages) elastic modulus (E_s) of 29.6×10^6 psi was placed between the platens in the machine. The apparent modulus E_m determined using the stiff machine instrumentation was found to be

$$E_m = 22.13 \times 10^6 \text{ psi.}$$

Substituting values of E_s , E_m , and the known modulus of the platen $E_p = 29.6 \times 10^6$ psi into equation (12) one finds that

$$A = 0.337.$$

From equation (7) one finds that

$$l_p = 1.348 \text{ in.}$$

This value was substantiated by additional tests using brass and aluminum cylinders. The sample deformation can then be obtained at any particular stress level by subtracting the quantity Δl_p from the total deformation (Δl).

$$\Delta l_p = \frac{l_p \sigma}{E_p}$$

where σ is the total force divided by the area of the platens. The quantities l and σ can be determined from the calibration curves in Diagrams A-1 and A-2.

In practice, the sample force-deformation (stress-strain) curve is derived from the experimental curve by making these point wise corrections.

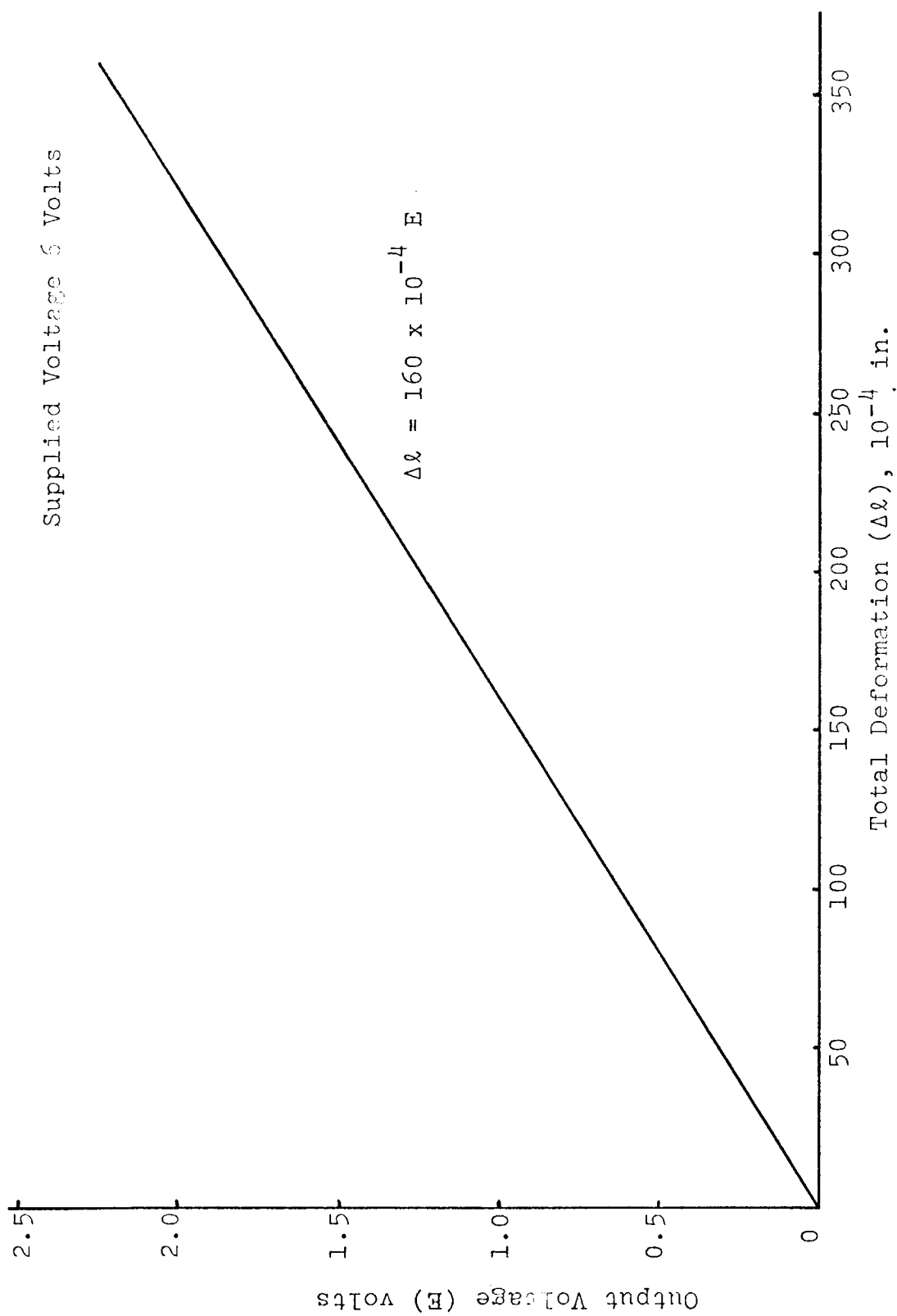


Diagram A-1. Calibration curve of the two DCDTs.

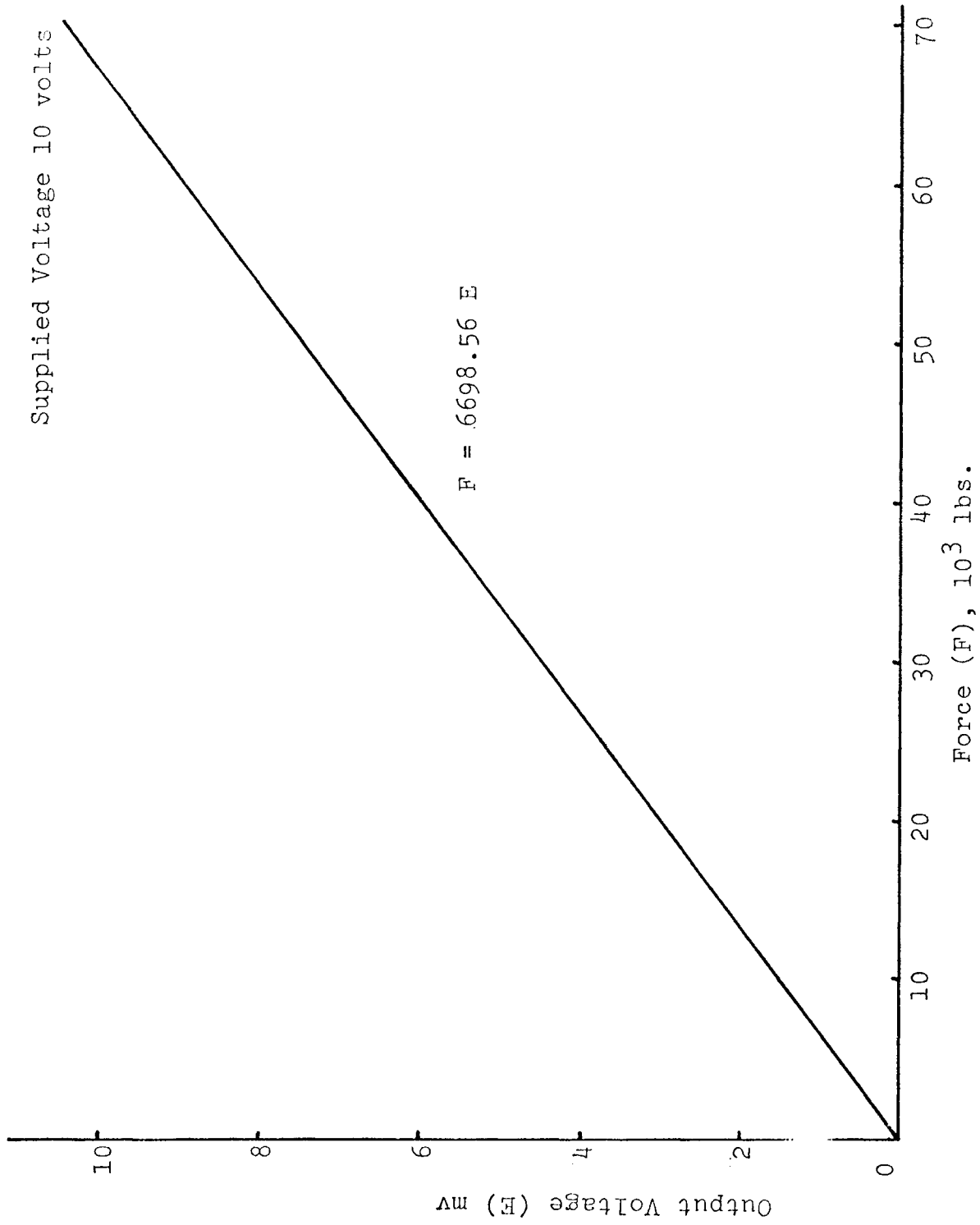


Diagram A-2. Calibration curve of the load cell.

APPENDIX B

§

```

C*****
C
C   COMPUTER PROGRAM FOR STIFFNESSES IN A RIB PILLAR MINE
C   PROGRAM WRITTEN BY FRANKLIN ROBINSON
C   MINING ENGINEERING DEPT.
C   THE ENTIRE MINE MUST BE DIVIDED IN STRIPS. THE STRIPS MUST
C   BE NUMBERED WITH THE IPIL IDENTIFICATION.
C*****
C
C   READ DATA
C   DIMENSION Z(60,60),S(60),IPIL(60),P(3600),B(60),
1  STIFF(60),C(60),STRESS(60),
2  DS(60)
   EPS=1.0E-8
   MAXIT=500
   READ(1,10)N,JQ
10  FORMAT(2I)
C
C   N IS THE NUMBER OF STRIPS IN THE MINE.
C   JQ IS THE NUMBER OF STRIPS IN THE ABUTMENT.
C
C   READ(1,5)(IPIL(L),L=1,N)
5   FORMAT(5I)
C
C   DELTA IS THE DIFFERENTIAL DISPLACEMENT TO FIND THE MINE
C   STIFFNESS.
C   DX IS THE HALF WIDTH OF THE STRIP.
C   T IS THE HEIGHT OF THE SEAM.
C   COMPST IS THE COMPRESSIVE STRENGTH OF THE PILLARS.
C
C   READ(1,13)E,ES,EP,POISSO,DELTA,DX,T,COMPST,Q
13  FORMAT(9F)
   A=E/(2.*3.1416*(1.-POISSO**2)*DX)
C
C   IPIL(L)=1 IS FOR PILLARS, AND IPIL(L)=2 IS FOR ROOMS
C   CALCULATION OF DISPLACEMENTS FOR EQUILIBRIUM
C   1 CONDITIONS
C
3   DO 1 J=1,N
     IR=IPIL(J)
     IF(IR.EQ.1)GO TO 200
     B(J)=-Q
     DO 2 K=1,N
2    Z(J,K)=A/(4.*(J-K)**2-1.)
     GO TO 1
*

```

```

      $
200   DO 4 K=1,N
      Z(J,K)=A/(4.*(J-K)**2-1.)
      IF(J.EQ.K)Z(J,K)=Z(J,K)-ES/T
4     CONTINUE
      B(J)=0.0
1     CONTINUE
      CALL SEIDEL(N,Z,B,S,EPS,MAXIT)
      WRITE(2,7)(S(K),K=1,N)
7     FORMAT(10X,4(E10.3,2X))
C
C     S ARE THE STRIPS DISPLACEMENTS
C     C ARE THE INDUCED STRESSES.

C     CALCULATION OF INDUCED STRESSES
C
      DO 14 J=1,N
      C(J)=0.0
      DO 11 K=1,N
11    C(J)=C(J)+(A/(4.*(J-K)**2-1.))*S(K)
14    CONTINUE
      WRITE(2,12)(C(J),J=1,N)
12    FORMAT(10X,4(F12.3,2X))
C
C     CALCULATION OF THE STIFFNESSES
C
      DO 20 I=N/2,N-JQ
      IR=IPIL(I)
      IF(IR.EQ.2)GO TO 20
50    DO 30 J=1,N
      IR=IPIL(J)
      IF(IR.EQ.1)GO TO 300
      B(J)=- (A/(4.*(J-I)**2-1.))*DELTA
      IF(J.EQ.I)B(J)=0.0
      DO 40 K=1,N
      Z(J,K)=A/(4.*(J-K)**2-1.)
      IF(J.EQ.I)Z(J,K)=0.0
      IF(K.EQ.I)Z(J,K)=0.0
40    CONTINUE
      GO TO 30
300   R=COMPST-Q
      B(J)=- (A/(4.*(J-I)**2-1.))*DELTA
      IF(J.EQ.I)B(J)=0.0
      DO 60 K=1,N
      Z(J,K)=(A/(4.*(J-K)**2-1.))
      IF(K.EQ.J)GO TO 130
      GO TO 140
130   Z(J,K)=Z(J,K)-ES/T
      *

```

```

$
IF(C(J).GE.R)Z(J,K)=(A/(4.*(J-K)**2-1.))-EP/T
140 IF(J.EQ.I)Z(J,K)=0.0
IF(K.EQ.I)Z(J,K)=0.0
60 CONTINUE
30 CONTINUE
100 L=1
DO 70 K=1,N
DO 80 J=1,N
P(L)=Z(J,K)
80 L=L+1
70 CONTINUE
K=1
DO 72 L=1,N*N
IF(P(L).EQ.0)GO TO 72
P(K)=P(L)
K=K+1
72 CONTINUE
K=1
DO 75 IQ=1,N-1
DO 76 J=1,N-1
Z(J,IQ)=P(K)
K=K+1
76 CONTINUE
75 CONTINUE
K=1
DO 73 J=1,N
IF(B(J).EQ.0)GO TO 73
B(K)=B(J)
K=K+1
73 CONTINUE
M=N-1
CALL SEIDEL(M,Z,B,DS,EPS,MAXIT)
STRESS(I)=0.0
K=1
600 IF(K.EQ.I)GO TO 500
STRESS(I)=STRESS(I)+(A/(4.*(I-K)**2-1.))*DS(K)
K=K+1
GO TO 600
500 STRESS(I)=STRESS(I)+(A/(4.*(I-K)**2-1.))*DELTA
IF(K.EQ.N)GO TO 800
DO 700 K=I+1,N
700 STRESS(I)=STRESS(I)+(A/(4.*(I-K)**2-1.))*DS(K-1)
800 STIFF(I)=T*STRESS(I)/DELTA
WRITE(2,160)I,STIFF(I)
C
C STIFF IS THE MINE STIFFNESS.
C
160 FORMAT(10X,I10,F15.2)
20 CONTINUE
STOP
END

```

#

```

$
C   GAUSS SEIDEL METHOD FOR SOLVING SIMULTANEEOUS
C   EQUATIONS
C   SUBROUTINE SEIDEL(N,A,B,X,EPS,MAXIT)
C   DIMENSION A(60,60),B(60),X(60)
C   BEGIN THE ITERATION SCHEME
C   ITER=1
C   STATEMENT 99 IS EXECUTED ONCE PER SWEEP
99  BIG=0.0
C   INDEX I SELECTS A ROW
C   DO 100 I=1,N
C   STATEMENT 102 IS EXECUTED ONCE PER ROW
102 SUM=0.0
C   SEGMENT FROM HERE THROUGH STATEMENT 107 GETS THE
C   SUM OF THE TERMS
C   IN A ROW , EXCLUDING THE MAIN DIAGONAL TERM
C   IF(I.EQ.1)GO TO 105
C   LAST=I-1
C   DO 106 J=1,LAST
106  SUM=SUM+A(I,J)*X(J)
C   IF(I.EQ.N)GO TO 103
105  INITL=I+1
C   DO 107 J=INITL,N
107  SUM=SUM+A(I,J)*X(J)
C   COMPUTE NEW VALUE OF A VARIABLE
103  TEMP=(B(I)-SUM)/A(I,I)
C   RESID=ABS(TEMP-X(I))
C   AT THE END OF SWEEP,THIS STATEMENT HAS PUT LARGEST
C   RESIDUAL IN BIG
C   IF(RESID.GT.BIG)BIG=RESID
100  X(I)=TEMP
C   ONE SWEEP HAS NOW BEEN COMPLETED
C   IF LARGEST RESIDUAL IS LESS THAN EPSILON,PROCESS
C   HAS CONVERGED
C   IF(BIG.LT.EPS)GO TO 30
C   IF ITERATION COUNTER EXCEEDS MAXIMUM ALLOWABLE
C   GIVE UP
C   IF(ITER.GE.MAXIT)GO TO 30
C   ITER=ITER+1
C   GO TO 99
30  WRITE(2,992)ITER
992  FORMAT(5H ITER,10X,15)
C   RETURN
C   END
*
```